

Perspective picture from Visual Sphere: *a new approach to image rasterization*

Jakub Maximilian Fober *

October 20, 2020

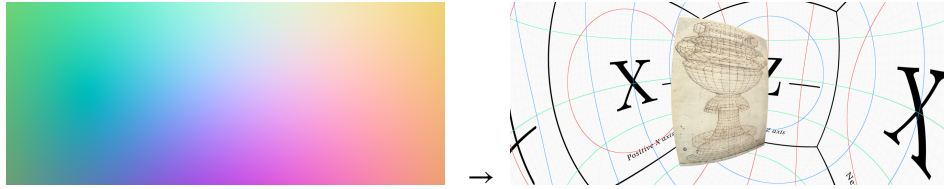


Figure 1: Example of aliasing-free, single-pass rasterization of polygon quad in real-time, from perspective vector map, where $\Omega^d = 270^\circ$, $k = 0.32$, $l = 62\%$, $s = 86\%$.

Abstract

In this paper alternative method for real-time 3D model rasterization is given. Surfaces are drawn in perspective-map space which acts as a virtual camera lens. It can render single-pass 360° angle of view (AOV) image of unlimited shape, view-directions count and unrestrained projection geometry (e.g. direct lens distortion, projection mapping, curvilinear perspective), natively aliasing-free. In conjunction to perspective vector map, visual-sphere perspective model is proposed. A model capable of combining pictures from sources previously incompatible, like fish-eye camera and wide-angle lens picture. More so, method is proposed for measurement and simulation of a real optical system variable no-parallax point (NPP). This study also explores philosophical and historical aspects of picture perception and presents a guide for perspective design.



*talk@maxfober.space

*https://maxfober.space

*https://orcid.org/0000-0003-0414-4223

Introduction

There is a great demand for perspective projection model able to produce computer-generated (CG) image up to 360° of view, with lens-distortions, directly from three-dimensional space, to pixel data. Currently there is no practical direct method for rasterization of real-time graphics in curvilinear perspective.²⁰ Every real-time perspective imagery incorporates *Pinhole Camera* model as a base, some with additional layers of distortion on top. Also knowledge about relationship between motion and perspective has not been properly formulated, leaving void in that field of image science. This paper aims at solving those issues. Study presents new, universal model for perspective projection and rasterization in CG graphics. It also explores history of perspective picture, redefines abstract theorem of image (as recorded in common-knowledge) and establishes rules for picture's perspective design.

This paper begins with a brief introduction to the visual-sphere perspective and jumps right into technical details of rasterization. If one is not familiar with the topic or terms, *Appendix* on page 27 gives great introduction and presents some basic knowledge on picture, perspective and perception, along with brief history of the topic. If one is familiar with this work and looks for some reference, Section 2 on page 16 presents algorithms of various perspective maps, used in visual-sphere rasterization. Within that, subsection 2.1 on page 16 presents *Universal Perspective* model. It describes variable image geometry in common projections. Variable (or floating) no-parallax point of real optical systems is described in section 3 on page 26. Additional figures are presented at the end of the document. At the very end of this document are code listings in GLSL for most of presented equations.

If one is looking for some artistic view on the topic, I recommend *Conclusion* on page 36 and some content from *Appendix* with Chapter's 1 introduction.

I hope that this work will bring a new breath into image production, open minds and possibilities for creative action and thinking.

Contents

1	on Visual Sphere perspective	6
1.1	Rasterization with perspective map	7
1.1.1	Aliasing-free step function	8
1.1.2	Miter mask for AA	9
1.1.3	Matrix rasterization	10
1.1.4	Interpolation in Fragment Shader	11
1.1.5	Perspective shader pass	12
1.2	Wire-frame rasterization	13
1.3	Simple particle rasterization	14
1.4	Hidden surface problem	15
2	Perspective picture transformations	16
2.1	Universal perspective	16
2.1.1	Parameters and limits	17
2.1.2	2D–3D transformation	18
2.1.3	3D–2D transformation	18
2.1.4	2D–2D transformation	19
2.2	Various projections	20
2.2.1	Rectilinear perspective	20
2.2.2	Curved panorama	20
2.2.3	Full dome	21
2.2.4	Equirectangular projection	21
2.2.5	Mirror dome projection	22
2.2.6	Projection mapping	23
2.2.7	Cube-mapping	24
2.2.8	Multiple-screen array	24
2.2.9	Virtual reality	25
2.3	Lens distortions	26
3	Variable no-parallax point	26
4	Appendix	27
4.1	Symbolic picture	29
4.2	Visual Sphere	30
4.2.1	Azimuthal projections	30
4.3	Motion and perspective	31
4.3.1	Attention focusing	32
4.3.2	in motion	33
4.4	History of the topic	34
5	Conclusion	36
	Acknowledgments	37

References	42
-------------------	-----------

License notice	45
-----------------------	-----------

List of Figures

1	Rasterized polygon example	1
2	Visual sphere model	6
3	Visual sphere coordinates	7
4	Aliasing-free step function	9
5	Rasterization masks in RGB	10
6	Barycentric coordinates in RGB	11
7	Simple particle model	14
8	Curved panorama	20
9	Mirror dome projection	22
10	Projection mapping	23
11	Cube map	24
12	Screen array	24
13	Virtual Reality	25
14	Radial compression charts	28
15	Motion in various azimuthal projections	32
16	View orientation and perspective	34
17	Anamorphic lens picture example	35
18	Rasterization examples	38
19	Vertex rasterization process flowchart	39
20	Fragment rasterization process flowchart	40
21	Floating no-parallax point	41

Listings

1	Pixel step function	45
2	Miter mask for aliasing-free rasterization	46
3	Aliasing-free rasterization	47
4	Aliased (jagged) rasterization	47
5	Barycentric coordinate interpolation vector	48
6	Aliasing-free wireframe	49
7	Aliased (jagged) wireframe	49
8	Particle rasterization	50
9	Fragment data occlusion	50
10	Screen coordinates transformation	51
11	Perspective parameters limiting	52
12	Universal perspective map	53
13	Rectilinear map	54

14	Curved panorama map	54
15	Full dome map	55
16	Equirectangular map	55
17	Mirror dome map	56
18	Projection-mapping map	57
19	Horizontal screen array map	58
20	Virtual reality map	58
21	View coordinates lens distortion	59

1 From Visual Pyramid to Visual Sphere

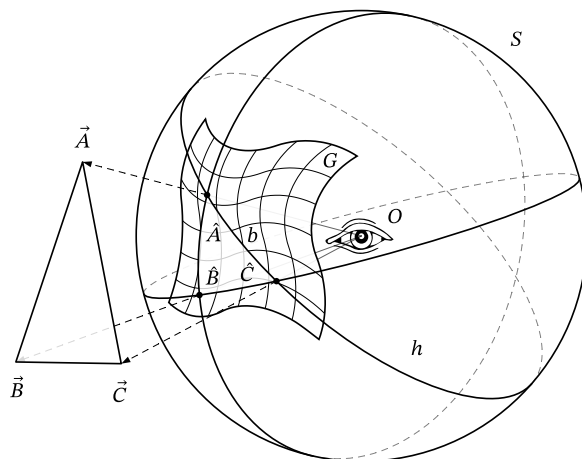


Figure 2: Projection of triangle \overline{ABC} onto visual unit sphere S , where projection origin O is at the sphere center. Edge of the projected triangle is always produced by an arc of a great circle, here $\overline{AC} \mapsto b \in h$. Grid G represents visual sphere vector map, where each pixel color is a spherical unit vector.

Visual pyramid of ALBERTI theorem¹ is by definition restricted to acute angles, which is limiting in terms of describable projections. This property makes stitching or layering multiple pictures defined in such space a problematic task. In the standard perspective model, introduced by L.B. ALBERTI, 3D point position is transformed into 2D plane/screen coordinates. Noticeably in some curvilinear projections, points are stretched into lines (see example 2 on page 17), making single visible point appear in multiple spots on picture plane/screen. This makes linear $3D \mapsto 2D$ point position mapping insufficient.

In the proposed visual-sphere model, every visible point in perspective picture's space has its own spherical position coordinate. Thus single point of a visual sphere can occupy multiple places in the picture, which conforms to this principle of curvilinear perspective. Such perspective space (a sphere) allows for stitching, layering and mapping of images in any single-point projection and perspective geometry.

Points in spherical projection model are no longer transformed into screen space. Rather lines are calculated and combined forming a polygon image (see figure 2). Straight line projected through the center point O will always form an arc of a great circle h . Such great circle can be mapped onto visual sphere described by incident vector map (later referred as *perspective map*). This process involves rotating the perspective map vector data. Goal is to align one of the axis of the map G with a great circle forming polygon edge (see figure 2). One way to rotate axis component is to calculate dot product between the perspective

vector map G and a unit vector perpendicular to points forming polygon edge, like $\|\vec{C} \times \vec{A}\|$ and the great circle h .

This process is essentially a half-space rasterization technique,²⁴ extended to spherical space.

1.1 Rasterization of the \overline{ABC} polygon triangle using \hat{G} vector from perspective map

Projected polygon geometry is always part of a great circle. The goal of the algorithm is to rasterize polygon shape formed by those spherical lines. Rasterization process involves determining orientation of the great-circle. Then rotating perspective map, so that the vertical axis of the map aligns with a great-circle. Next the step-function is performed on a \vec{G}'_i component of the rotated vector map G' . The step function algorithm is essential for aliasing-free edge rasterization. Full n -sided convex polygon picture is defined by intersection of n -number of such operations.

$$\begin{bmatrix} \vec{G}'_1 \\ \vec{G}'_2 \\ \vec{G}'_3 \end{bmatrix} = \begin{bmatrix} \hat{G} \cdot \|\vec{A} \times \vec{B}\| \\ \hat{G} \cdot \|\vec{B} \times \vec{C}\| \\ \hat{G} \cdot \|\vec{C} \times \vec{A}\| \end{bmatrix} \quad (1a)$$

$$\overline{ABC} \mapsto G = \min \{ \text{step}(\vec{G}'_1), \text{step}(\vec{G}'_2), \text{step}(\vec{G}'_3) \} \quad \blacksquare \quad (1b)$$

Rotation of perspective map vector \hat{G} is performed with a dot product between each \hat{G} and rotation-direction vector. Which is a dot product between perspective map G and normalized cross product of two edge points. Rotation vector doesn't have to be normalized, but that could cause some precision errors, especially when using aliasing-free step function.

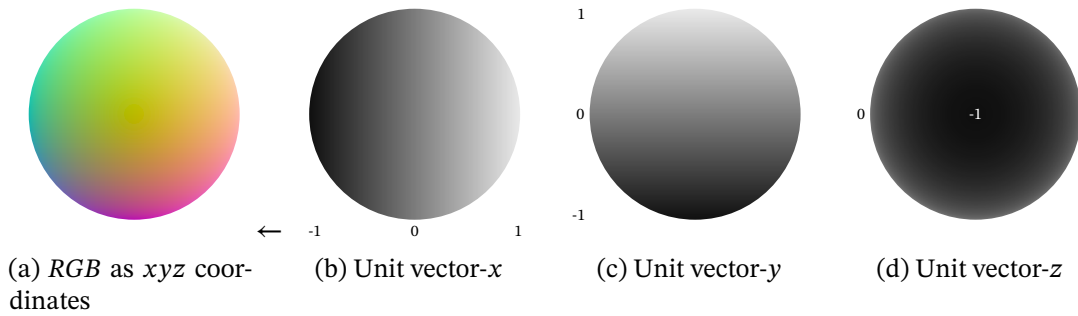


Figure 3: Visual sphere in vector coordinates as seen from outside, facing Z direction. Each vector component x , y and z can be rotated independently.

Visual sphere perspective model is ultimately a *cosine*-based perspective model and can produce pictures in both *tangent perspective* and *sine perspective*. As seen in figure 3, each sphere surface point has a value associated to its position. Those

three values also represent cosine of an angle between axis vectors $[1 \ 0 \ 0]$, $[0 \ 1 \ 0]$, $[0 \ 0 \ 1]$ and the surface position vector. After rotation of \hat{G} , those three axes are represented by rotation matrix vectors.

1.1.1 Aliasing-free step function

Step function is performed on rotated \vec{G}' coordinate and determines inside and outside of a polygon for each edge. Aliasing-free result can be achieved by changing width of the step-function slope from binary, to one-pixel wide (see figure 4 on the following page). Below presented are two algorithms for a step function.

$$\text{pstep}(g) = \left\{ \frac{g}{\partial(g)} + \frac{1}{2} \right\} \cap [0, 1] \quad (2a)$$

$$\text{bstep}(g) = \begin{cases} 1, & \text{if } g > 0 \\ 0, & \text{otherwise} \end{cases} \quad (2b)$$

$\text{pstep}(g)$ function (p standing for *pixel*) gives smooth aliasing-free result. The $\text{bstep}(g)$ function is a binary operation and gives aliased output. $\partial(x)$ function is an equivalent to ***fwidth***(x) GLSL function. $1/2$ offset centers anti-aliasing gradient at the polygon edge (as seen in subfigure 4c compared to subfigure 4a on the next page).

Global delta δ can replace denominator $\partial(g)$ in $\text{pstep}()$ function. It gives more natural look and has smaller computational footprint. Global delta δ is derived from perspective vector map \hat{G} . Its value can be preprocessed and saved in a texture. The difference between preprocessed delta δ and per-fragment ∂ is in polygon-edge slope width.

$$\delta = \frac{1}{\max \{ \partial(\hat{G}_x), \partial(\hat{G}_y), \partial(\hat{G}_z) \}} \quad (3a)$$

$$\text{gpstep}(g) = \left\{ \delta g + \frac{1}{2} \right\} \cap [0, 1] \quad (3b)$$

The result of δ calculation is a single-channel texture, which represents reciprocal of the component-wise maximum ***fwidth***(x) of perspective map vector \hat{G} .

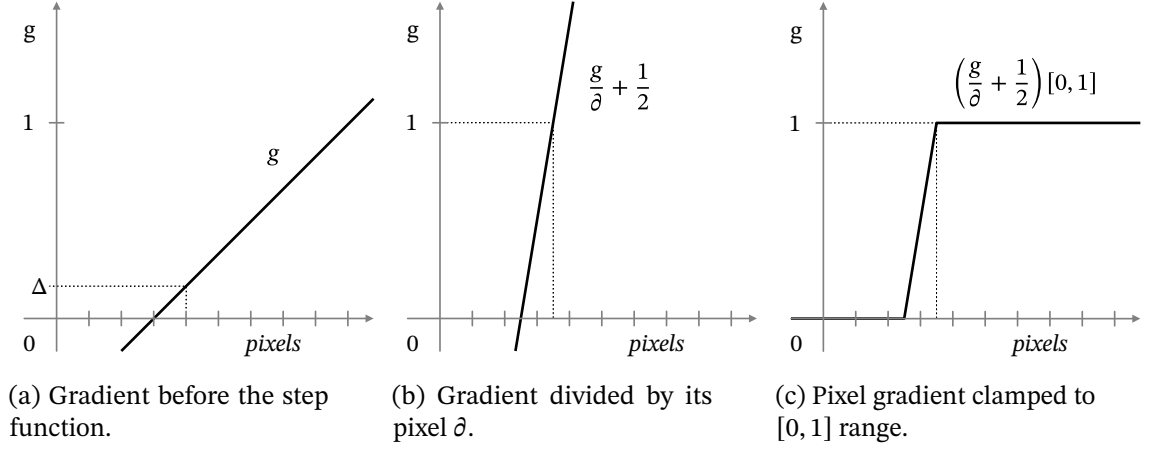


Figure 4: Aliasing-free step function process, where g is the gradient function. δ is equivalent of $\text{fwidth}(g)$ GLSL function. Horizontal axis represents pixel position and vertical, the value of g .

Remark. When combining polygons into polygon-strip using pixel-step function, it is important to sum each mask, otherwise visible seam may occur. See more on combining fragments into buffer in subsection 1.4 on page 15.

1.1.2 Miter mask for pixel-step rasterization

In special case, when projected polygon's edges meet at very shallow angle, corners will extend beyond polygon outline (due to half-pixel offset in the $\text{pstep}(g)$ function). This visual artifact can be corrected by a miter mask. There are many ways to calculate such mask, one is to define the smallest circle over projected triangle. Following algorithm uses barycentric coordinates to determine the smallest circle's center and size.¹¹

$$\begin{cases} a^2 = |\hat{B} - \hat{C}|^2 = (\hat{B} - \hat{C}) \cdot (\hat{B} - \hat{C}) \\ b^2 = |\hat{C} - \hat{A}|^2 = (\hat{C} - \hat{A}) \cdot (\hat{C} - \hat{A}) \\ c^2 = |\hat{A} - \hat{B}|^2 = (\hat{A} - \hat{B}) \cdot (\hat{A} - \hat{B}) \end{cases} \quad (4a)$$

$$\begin{bmatrix} \vec{O}_s \\ \vec{O}_t \\ \vec{O}_p \end{bmatrix} = \begin{bmatrix} a^2(b^2 + c^2 - a^2) \\ b^2(c^2 + a^2 - b^2) \\ c^2(a^2 + b^2 - c^2) \end{bmatrix} \quad (4b)$$

$$\vec{S} = \begin{cases} 0.5(\hat{B} + \hat{C}), & \text{if } \vec{O}_s \leq 0 \\ 0.5(\hat{C} + \hat{A}), & \text{if } \vec{O}_t \leq 0 \\ 0.5(\hat{A} + \hat{B}), & \text{if } \vec{O}_p \leq 0 \\ \frac{\vec{O}_s \hat{A} + \vec{O}_t \hat{B} + \vec{O}_p \hat{C}}{\vec{O}_s + \vec{O}_t + \vec{O}_p}, & \text{otherwise} \end{cases} \quad (4c)$$

Where \vec{O} is the barycentric coordinate of circumcenter. a^2, b^2, c^2 are squared lengths of projected triangle's edges. \vec{S} is the smallest-circle center vector which length is equal to the cosine of an angle between \hat{S} and the smallest-circle rim. Polygon triangle is degenerate if $0 = \vec{O}_s + \vec{O}_t + \vec{O}_p$, meaning all projected $\hat{A}, \hat{B}, \hat{C}$ points lay in one line. In such case miter mask can be omitted. Having the smallest circle center vector \vec{S} , rasterization algorithm can be updated as follows:

$$\begin{bmatrix} \vec{G}'_1 \\ \vec{G}'_2 \\ \vec{G}'_3 \\ \vec{G}'_4 \end{bmatrix} = \begin{bmatrix} \hat{G} \cdot \|\vec{A} \times \vec{B}\| \\ \hat{G} \cdot \|\vec{B} \times \vec{C}\| \\ \hat{G} \cdot \|\vec{C} \times \vec{A}\| \\ \hat{G} \cdot \hat{S} - |\vec{S}| \end{bmatrix} \quad (5a)$$

$$\overline{ABC} \mapsto G = \min \{ \text{pstep}(\vec{G}'_1), \text{pstep}(\vec{G}'_2), \text{pstep}(\vec{G}'_3), \text{pstep}(\vec{G}'_4) \} \quad \blacksquare \quad (5b)$$

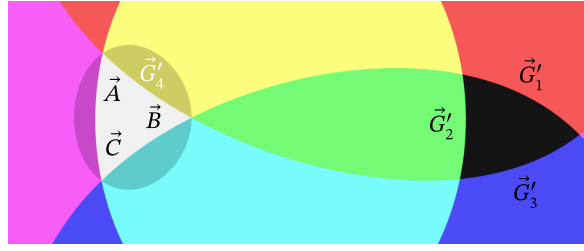


Figure 5: Rasterization masks as RGB values, where perspective map represents $\Omega^d = 270^\circ, k = 0.32, l = 62\%, s = 86\%$.

1.1.3 Rasterization using matrix multiplication

Since rasterization involves multiple dot products (equation 5a), part of the process can be mitigated to matrix multiplication, where each matrix row represents rotation vector. Such matrix is calculated once per polygon-per frame and is executed per fragment pixel. Full vertex rasterization process is presented on figure 19 on page 39.

$$\begin{bmatrix} \vec{G}'_1 \\ \vec{G}'_2 \\ \vec{G}'_3 \\ \vec{G}'_4 \end{bmatrix} = \begin{bmatrix} \hat{G}_x \\ \hat{G}_y \\ \hat{G}_z \end{bmatrix} \begin{bmatrix} \|\vec{A} \times \vec{B}\| \\ \|\vec{B} \times \vec{C}\| \\ \|\vec{C} \times \vec{A}\| \\ \hat{S}_x \hat{S}_y \hat{S}_z \end{bmatrix} - \begin{bmatrix} 0 \\ 0 \\ 0 \\ |\vec{S}| \end{bmatrix} \quad (6a)$$

$$\overline{ABC} \mapsto G = \min \{ \text{pstep}(\vec{G}'_1), \text{pstep}(\vec{G}'_2), \text{pstep}(\vec{G}'_3), \text{pstep}(\vec{G}'_4) \} \quad \blacksquare \quad (6b)$$

This procedure can be expanded to any convex n -sided planar polygon using procedural equation as follows:

$$\begin{bmatrix} \vec{G}'_1 \\ \vec{G}'_2 \\ \vdots \\ \vec{G}'_n \end{bmatrix} = \begin{bmatrix} \hat{G}_x \\ \hat{G}_y \\ \hat{G}_z \end{bmatrix} \begin{bmatrix} \|T_1 \times T_2\| \\ \|T_2 \times T_3\| \\ \vdots \\ \|T_n \times T_{(i+1) \bmod n}\| \end{bmatrix} \quad (7a)$$

$$\text{mask}(\vec{G}') = \min \{ \text{step}(\vec{G}'_1), \text{step}(\vec{G}'_2), \dots, \text{step}(\vec{G}'_n) \} \quad \blacksquare \quad (7b)$$

Here T describes n -sided polygon points $n \times 3$ matrix, where each row is a vertex position (counting clock-wise). Each rotation vector is derived from cross product between i -vertex and $i + 1$. For the the last n^{th} vertex, next one is $\mathcal{N} \oplus 1$.

1.1.4 Fragment data interpolation from barycentric coordinates

Rendering realistic polygon graphics involves shading and texture mapping. Values of normal, depth and UV coordinates associated to each vertex are interpolated across polygon surface using barycentric coordinate of the fragment point.

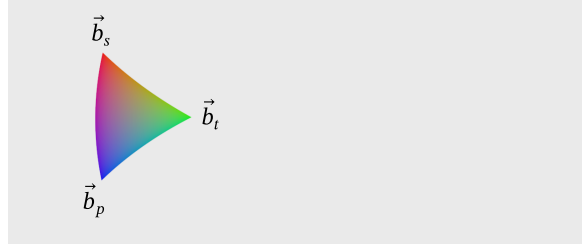


Figure 6: Barycentric coordinates as RGB values. Here perspective map represents $\Omega^d = 270^\circ$, $k = 0.32$, $l = 62\%$, $s = 86\%$.

$$\vec{N} = \begin{cases} (\vec{A} - \vec{B}) \times (\vec{C} - \vec{B}) \\ (\vec{B} - \vec{C}) \times (\vec{A} - \vec{C}) \\ (\vec{C} - \vec{A}) \times (\vec{B} - \vec{A}) \end{cases} \quad (8)$$

Normal vector $\vec{N} \in \mathbb{R}^3$ of the triangle plane \overline{ABC} is derived from cross product between two triangle edges. Length of this vector is equal to the area of a parallelogram formed by those two edges, which is equal to double the area of

triangle \overline{ABC} .

$$r = \frac{\vec{A} \cdot \vec{N}}{\hat{G} \cdot \vec{N}} = \frac{\vec{B} \cdot \vec{N}}{\hat{G} \cdot \vec{N}} = \frac{\vec{C} \cdot \vec{N}}{\hat{G} \cdot \vec{N}} \quad (9a)$$

$$\equiv |\hat{G} \rightarrow \overline{ABC}| \quad (9b)$$

Distance r represents multiplier of the visual sphere vector \hat{G} , to intersection point on the \overline{ABC} triangle plane. Since \hat{G} is a unit vector, value r can be exported as depth (representing distance, not z -position). Here vector \vec{A} , \vec{B} , \vec{C} in the numerator can be replaced by any point on the triangle plane.

$$\begin{bmatrix} \vec{b}_s \\ \vec{b}_t \\ \vec{b}_p \end{bmatrix} = \begin{bmatrix} |(\vec{B} - r\hat{G}) \times (\vec{C} - r\hat{G})| \\ |(\vec{C} - r\hat{G}) \times (\vec{A} - r\hat{G})| \\ |(\vec{A} - r\hat{G}) \times (\vec{B} - r\hat{G})| \end{bmatrix} \div |\vec{N}| \quad (10a)$$

Since $\vec{A} \cdot \vec{B} = |\vec{A}||\vec{B}| \cos \alpha$ and $\overline{AB} \perp (\vec{A} \times \vec{B})$ this equation can be rewritten using triple product, as follows.

$$\begin{bmatrix} \vec{b}_s \\ \vec{b}_t \\ \vec{b}_p \end{bmatrix} = \begin{bmatrix} (\vec{C} - r\hat{G}) \times (\vec{B} - r\hat{G}) \cdot \vec{N} \\ (\vec{A} - r\hat{G}) \times (\vec{C} - r\hat{G}) \cdot \vec{N} \\ (\vec{B} - r\hat{G}) \times (\vec{A} - r\hat{G}) \cdot \vec{N} \end{bmatrix} \div (\vec{N} \cdot \vec{N}) \quad (11a)$$

Barycentric vector \vec{b} is a proportion of surface area. From vector \vec{b} , various vertex properties are interpolated (e.g. depth, normal vector and texture coordinates), given each vertex A , B and C has an associated value.

$$f_r = r \quad (12a)$$

$$f_{\vec{N}} = \|\vec{b}_s A_{\vec{N}} + \vec{b}_t B_{\vec{N}} + \vec{b}_p C_{\vec{N}}\| \quad (12b)$$

$$f_{\vec{f}} = \vec{b}_s A_{\vec{f}} + \vec{b}_t B_{\vec{f}} + \vec{b}_p C_{\vec{f}} \quad (12c)$$

Interpolation of fragment data f is done through a dot product between barycentric coordinate vector \vec{b} and values associated to each vertex. Here f_r is the depth pass (representing distance, not z -position), $f_{\vec{N}}$ is the interpolated normal vector and $f_{\vec{f}}$ are the texture coordinates. All interpolations are perspective-correct. Figure 20 on page 40 shows this process in a step-by-step flowchart.

1.1.5 Perspective pixel-shader pass

Prior to geometry rasterization, pixel perspective shader pass may be performed. Its output works as a perspective vector map. This pipeline addition enables special effects like dynamic perspective and projection mapping, flat mirror reflection, screen-space refraction (e.g. concave refractive surfaces which expand AOV), etc.

Example 1. Projection mapping with dynamic view-position can be achieved by transforming vector data of world-position-pass texture S . Knowing viewer position \vec{O} , offset can be applied to \vec{S} . When normalized, \hat{S}' produces perspective map vector $\hat{G} = \|\vec{S} - \vec{O}\|$. Complexity of projection surface and number of views (used projectors) is outside of concern, as view-position transformation is performed on a baked texture. Exact formula for projection mapping is available in sub-subsection 2.2 on page 20.

1.2 Wire-frame line segment rasterization

It is possible to produce screen-relative line drawing based on a perspective map. Following algorithm will produce wire-frame image of projected \overline{AB} line segment.

$$\vec{G}'_z = \hat{G} \cdot \|\vec{A} \times \vec{B}\| \quad (13)$$

Perspective vector map component \hat{G}_z is rotated by \overline{ABO} tangent vector $\|\vec{A} \times \vec{B}\|$, where \vec{O} is the observation point.

$$\text{blstep}(\vec{G}'_z) = \begin{cases} 1, & \text{if } \partial(\vec{G}'_z) - |2\vec{G}'_z| > 0 \\ 0, & \text{otherwise} \end{cases} \quad (14a)$$

$$\text{plstep}(\vec{G}'_z) = 1 - \min \left\{ \frac{|\vec{G}'_z|}{\partial(\vec{G}'_z)}, 1 \right\} \quad (14b)$$

Above is a line-step function in two variants, binary-aliased (14a) and pixel-smooth (14b). $\partial(x)$ is equivalent to **fwidht**(x) function of GLSL.

$$\vec{L} = \frac{\vec{A} + \vec{B}}{2} \quad (15a)$$

$$h = \text{lstep}(\vec{G}'_z) \quad (15b)$$

$$l = \min \{ \text{step}(\hat{G} \cdot \vec{L} - |\vec{L}|), h \} \quad \blacksquare \quad (15c)$$

Radial mask combined with great circle h forms \overline{AB} line segment image l . \vec{L} is the line-middle vector, $\text{lstep}(\vec{G}'_z)$ function rasterizes great-circle h . Radial mask is formed by the $\text{step}(x)$ function of dot product between perspective map vector \hat{G} and line-middle vector \vec{L} , minus $|\vec{L}| = \cos \theta/2$.

1.3 Simple procedural particle rasterization

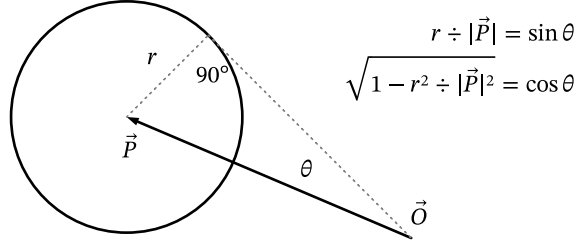


Figure 7: Simple particle model, where r is the particle radius and \vec{P} is the particle position from observation point \vec{O} .

Following algorithm will produce mask image of spherical particle, given position and radius.

$$\text{particle}(\hat{G}, \vec{P}, r) = \text{step} \left(\hat{G} \cdot \hat{P} - \sqrt{1 - r^2 \div (\vec{P} \cdot \vec{P})} \right) \quad (16)$$

Where $\vec{P} \in \mathbb{R}^3$ is the particle position. r is particle radius and \hat{G} is the perspective map vector. To obtain texture coordinates within the particle, following algorithm can be used.

$$\hat{X} = \|\vec{P}_z, 0, -\vec{P}_x\| \quad (17a)$$

$$\hat{Y} = \|\hat{X} \times \vec{P}\| \equiv \hat{X} \times \hat{P}$$

$$\begin{bmatrix} \vec{f}_s^P \\ \vec{f}_t^P \end{bmatrix} = \begin{bmatrix} \hat{G}_x \\ \hat{G}_y \\ \hat{G}_z \end{bmatrix} \begin{bmatrix} \hat{X}_x & \hat{X}_y & \hat{X}_z \\ \hat{Y}_x & \hat{Y}_y & \hat{Y}_z \end{bmatrix} \frac{|\vec{P}|}{2r} + \frac{1}{2} \quad \blacksquare \quad (17b)$$

Where \vec{f}^P is the texture coordinate of the particle, \hat{X} and \hat{Y} are rotation matrix vectors. Full particle rasterization process with texture coordinates and round mask can be described by following algorithm.

$$\begin{bmatrix} \vec{G}'_1 \\ \vec{G}'_2 \\ \vec{G}'_3 \end{bmatrix} = \begin{bmatrix} \hat{G}_x \\ \hat{G}_y \\ \hat{G}_z \end{bmatrix} \begin{bmatrix} \|\vec{P}_z, 0, -\vec{P}_x\| \\ \|\vec{P}_z, 0, -\vec{P}_x\| \times \hat{P} \\ \hat{P}_x & \hat{P}_y & \hat{P}_z \end{bmatrix} \quad (18a)$$

$$m^P = \text{step} \left(\vec{G}'_3 - \sqrt{1 - r^2 \div (\vec{P} \cdot \vec{P})} \right) \quad \blacksquare \quad (18b)$$

$$\begin{bmatrix} \vec{f}_s^P \\ \vec{f}_t^P \end{bmatrix} = \begin{bmatrix} \vec{G}'_1 \\ \vec{G}'_2 \end{bmatrix} \frac{|\vec{P}|}{2r} + \frac{1}{2} \quad \blacksquare \quad (18c)$$

Where $\vec{f}^P \in [0, 1]^2$ are the texture coordinates, $m^P \in [0, 1]$ is the particle mask, \vec{P} is the particle position with r as radius. \hat{G} is the perspective-map vector.

1.4 Hidden surface occlusion

One of the key features of 3D polygon rasterization is hidden surface occlusion (HSO). There are many approaches that solve HSO problem. One of them is depth-pass test, where each depth r of the fragment pixel is tested against already rasterized geometry depth r^\perp . This simple technique works well with the binary step function (see sub-subsection 1.1.1 on page 8). Depth pass test technique produces aliased result with some pixels being drawn multiple times during a single pass.

To utilize advantage of aliasing-free rasterization in perspective map rasterization, geometry data should be rasterized in a very organized order. Optimal approach is to render scene front-to-back and discard already painted pixels during polygon mask rasterization. Such ordered rasterization can be achieved with binary space partitioning^{13,22} (BSP) and concurrent binary trees¹⁰ (CBT). This solution produces aliasing-free result, without depth-buffer check. It paints pixels only once for most of the time.

$$\begin{cases} m^{fc} = \min\{m^f, 1 - m^b\} \\ m = m^b + m^{fc} \end{cases} \quad (19)$$

Above equation combines fragment data with the buffer mask in front-to-back rasterization. Where m^f is the currently processed fragment black-and-white mask. m^b is the buffer mask of already rasterized geometry. Mask m^{fc} is the fragment mask clipped (occluded) by the buffer mask m^b . Simple addition combines current fragment mask m^{fc} with the buffer m^b . Same addition can be performed for any fragment data, having the m^{fc} as a mask. For example UV coordinates for surface textures (equation 20b), normal pass (equation 20c), depth pass (equation 20a), etc. Initial value of each buffer is equal zero.

$$r = m^{fc}r^f + r^b, \quad r^b(1) = 0 \quad (20a)$$

$$\vec{f} = m^{fc}\vec{f}^f + \vec{f}^b, \quad \vec{f}^b(1) = [0 \ 0]^T \quad (20b)$$

$$\hat{N} = \|m^{fc}\hat{N}^f + \hat{N}^b\|, \quad \hat{N}^b(1) = [0 \ 0 \ 0]^T \quad (20c)$$

Where r is the depth pass, $\vec{f} \in [0, 1]^2$ represents texture coordinates and $\hat{N} \in [0, 1]^3$ is the normal vector. Current fragment mask (occlusion clipped) is denoted by m^{fc} . “ f ” in a superscript indicates current fragment data and “ b ” in superscript–buffer data of already rasterized geometry. Initial values of the buffer are denoted by “(1)” in suffix.

2 Perspective transformations of 2D/3D data

In this section presented algorithms produce perspective picture from 3D and 2D data. Most of them describe 2D→3D transformation, which outputs perspective vector map from texture coordinates, suitable for rasterization.

Remark. For a proper transformation, 2D coordinates must be normalized for a given AOV type (e.g. vertical, diagonal or horizontal).

Example. For a pixel i in picture of aspect-ratio 16:9 and horizontal-AOV, coordinates (i_x, i_y) must be centered and horizontally normalized, so that $i_x \in [-1, 1]$ and $i_y \in \left[-\frac{9}{16}, \frac{9}{16}\right]$.

$$\begin{bmatrix} \vec{f}_x \\ \vec{f}_y \end{bmatrix} = \left(2 \begin{bmatrix} \vec{f}_s \\ \vec{f}_t \end{bmatrix} - 1 \right) \begin{cases} \begin{bmatrix} 1 & 1 \\ a & a \end{bmatrix}^T, & \text{if } \Omega \text{ horizontal} \\ \begin{bmatrix} a & 1 \\ 1 & 1 \end{bmatrix}^T, & \text{if } \Omega \text{ vertical} \\ \begin{bmatrix} a & 1 \\ 1 & 1 \end{bmatrix}^T \div \sqrt{1+a^2}, & \text{if } \Omega \text{ diagonal} \\ \begin{bmatrix} a & 1 \\ 1 & 1 \end{bmatrix}^T \div \frac{4}{3}, & \text{if } \Omega \text{ horizontal } 4 \times 3 \end{cases} \quad (21)$$

Above are view coordinates $x, y \in [-1, 1]$ from texture coordinates $s, t \in [0, 1]$, where a is the picture aspect ratio and Ω is the AOV.

$$\begin{bmatrix} \vec{f}_s \\ \vec{f}_t \end{bmatrix} = \frac{1}{2} + \frac{1}{2} \begin{bmatrix} \vec{f}_x \\ \vec{f}_y \end{bmatrix} \begin{cases} \begin{bmatrix} 1 & a \\ a & a \end{bmatrix}^T, & \text{if } \Omega \text{ horizontal} \\ \begin{bmatrix} \frac{1}{a} & 1 \\ a & 1 \end{bmatrix}^T, & \text{if } \Omega \text{ vertical} \\ \begin{bmatrix} \frac{1}{a} & 1 \\ a & 1 \end{bmatrix}^T \sqrt{1+a^2}, & \text{if } \Omega \text{ diagonal} \\ \begin{bmatrix} \frac{1}{a} & 1 \\ a & 1 \end{bmatrix}^T \frac{4}{3}, & \text{if } \Omega \text{ horizontal } 4 \times 3 \end{cases} \quad (22)$$

Here are texture coordinates $s, t \in [0, 1]$ from view coordinates $x, y \in [-1, 1]$, where a is the picture aspect ratio and Ω is the AOV.

2.1 Universal perspective model

Universal perspective model allows for a smooth adjustment of image geometry in accordance to the visible content. Presented two transforms produce *perspective picture* (see definition on page 30). First 2D→3D transformation produces perspective vector in various common projections, which is suitable for generating universal-perspective maps for rasterization. Second 3D→2D transformation produces picture coordinates of various projections. Combination of both can map between different projections.

Remark. Note that 3D→2D transformation may be non-linear, meaning that a 3D vector can be represented by multiple 2D coordinates in very special cases.

Example 2. In *equidistant* projection at $\Omega = 2\pi$ (whole sphere) visible point opposite to the view direction is represented by a ring at the picture's boundary.

2.1.1 Universal perspective parameters and limits

There is total of four parameters defining perspective picture geometry in the universal perspective model.

angle Ω defines angle of view (AKA FOV), which varies between $\rightarrow \pi$ and 2π .

scalar k defines perspective type as a value in range $[-1, 1]$, which interpolates between various azimuthal projections:

<i>Gnomonic (rectilinear)</i>	$k = 1$
<i>Stereographic</i>	$k = 0.5$
<i>Equidistant</i>	$k = 0$
<i>Equisolid</i>	$k = -0.5$
<i>Orthographic</i>	$k = -1$

scalar l in range $[0, 1]$ defines cylindricity of the projection, where $l = 0$ represents cylindrical projection and $l = 1$ — spherical projection.

scalar s in range $[4/5, 1]$ defines vertical anamorphic correction of a non-spherical projection, meaning that it is only active when $l < 1$.

Base projection type is adjusted by the k component. It manipulates image perception. Cylindrical projection, is adjusted by the l component. Low l values should represent view at level (see subfigure 16a on page 34). For roll motion, recommended value for l is 100% (see subfigure 16b). Anamorphic correction of non-spherical image, driven by the s component, depends on subject in view. Purpose of the s scalar is to adjust proportions of the figure-in-focus.

$$\left\{ \begin{array}{l} \Omega_{\max} = \frac{1}{\max\{1/2, |k|\}} \cdot \begin{cases} \rightarrow \pi, & \text{if } k > 0 \\ \pi, & \text{otherwise} \end{cases} \\ \Omega \in (0, \Omega_{\max}] \\ k \in [-1, 1] \\ l \in [0, 1] \\ s \in [4/5, 1] \end{array} \right. \quad (23)$$

Limits for perspective parameters in universal perspective model. Value of Ω_{\max} depends on the projection type (represented by scalar k) and varies between angle approaching 180° and 360° angle.

2.1.2 Transformation of 2D→3D coordinates

This transformation produces visual sphere vector map from texture coordinates, that can be later used as an input for perspective map rasterizer.

$$R = \left\| \begin{bmatrix} \vec{f}_x \\ \vec{f}_y \cdot \sqrt{l} \end{bmatrix} \right\| \quad (24a)$$

$$\equiv \sqrt{\vec{f}_x^2 + l\vec{f}_y^2} \quad (24b)$$

$$\theta = \begin{cases} \arctan \left(\tan \left(k \frac{\Omega}{2} \right) R \right) \div k, & \text{if } k > 0 \\ \frac{\Omega}{2}, & \text{if } k = 0 \\ \arcsin \left(\sin \left(k \frac{\Omega}{2} \right) R \right) \div k, & \text{if } k < 0 \end{cases} \quad (24c)$$

$$\begin{bmatrix} \hat{v}_x \\ \hat{v}_y \\ \hat{v}_z \end{bmatrix} = \left\| \begin{bmatrix} \vec{f}_x \\ \vec{f}_y \\ 1 \end{bmatrix} \begin{bmatrix} \sin(\theta)/R \\ \sin(\theta)/R \\ \cos \theta \end{bmatrix} \div \begin{bmatrix} 1 \\ l(1-s) + s \\ 1 \end{bmatrix} \right\| \quad \blacksquare \quad (24d)$$

Picture coordinates are denoted by vector $\vec{f} \in [0, 1]^2$, a is picture aspect ratio. Transformed 3D coordinates are represented by normalized vector $\hat{v} \in [-1, 1]^3$. Scalar k represents various projection types. Scalar $l \in [0, 1]$ is the spherical projection factor, with $l = 0$ representing cylindrical projection and $l = 1$, a spherical projection. Scalar $s \in [4/5, 1]$ describes anamorphic correction of non-spherical image. For $s = 1$ or $l = 1$ there is no anamorphic correction.

2.1.3 Transformation of 3D→2D coordinates

This transformation is mainly used in a pixel shader, where basic rectilinear projection can be mapped to spherical one. It is not suitable for mapping 3D points onto 2D picture plane as in some specific cases single 3D point can map to multiple 2D positions (see example 2 on the previous page).

$$\hat{v} = \begin{bmatrix} \hat{v}_x \\ \hat{v}_y \\ \hat{v}_z \end{bmatrix} \quad (25a)$$

$$\theta = \arccos \left(\hat{v}_z \div \sqrt{\hat{v}_x^2 + l\hat{v}_y^2 + \hat{v}_z^2} \right) \quad (25b)$$

$$R = \begin{cases} \tan(k\theta) \div \tan \left(k \frac{\Omega}{2} \right), & \text{if } k > 0 \\ \theta \div \frac{\Omega}{2}, & \text{if } k = 0 \\ \sin(k\theta) \div \sin \left(k \frac{\Omega}{2} \right), & \text{if } k < 0 \end{cases} \quad (25c)$$

$$\begin{bmatrix} \vec{f}_x \\ \vec{f}_y \end{bmatrix} = \begin{bmatrix} \hat{v}_x \\ \hat{v}_y \end{bmatrix} \frac{R}{\sqrt{\hat{v}_x^2 + l\hat{v}_y^2}} \begin{bmatrix} 1 \\ l(1-s) + s \end{bmatrix} \quad \blacksquare \quad (25d)$$

3D coordinates are represented by a normalized vector $\hat{v} \in [-1, 1]^3$, where view origin is at position $[0 \ 0 \ 0]$. Transformed picture coordinates are represented by vector $\vec{f} \in \mathbb{R}^2$, where image center is at position $[0 \ 0]$. Angle θ is between vector \hat{v} and the Z axis. R is the normalized distance between projected vector \vec{f} and the image center, where $\vec{f} \leftrightarrow \hat{v}$. Angle Ω is equal to AOV, where $\Omega_{\max} \in [\rightarrow \pi, 2\pi]$. Scalar k represents various projection types (see sub-subsection 2.1.1 on page 17). Scalar $l \in [0, 1]$ is the spherical projection factor, where $l = 0$ represents cylindrical projection and $l = 1$ represents spherical projection. Scalar $s \in [4/5, 1]$ describes anamorphic correction of non-spherical image. For $s = 1$ or $l = 1$ there is no anamorphic correction. This transformation is a reverse of the universal 2D \rightarrow 3D transform on the previous page.

2.1.4 Transformation of 2D \rightarrow 2D coordinates

Combination of 3D and 2D transformation can be used to map between two different projections, for example *stereographic* \leftrightarrow *equidistant*, using two separate perspective component sets, $\{\Omega_i, k_i, l_i, s_i\}$ and $\{\Omega_o, k_o, l_o, s_o\}$ for input and output picture.

$$R_i = \left\| \begin{bmatrix} \vec{f}_x \\ \vec{f}_y \cdot \sqrt{l_i} \end{bmatrix} \right\| \quad (26a)$$

$$\equiv \sqrt{\vec{f}_x^2 + l_i \vec{f}_y^2} \quad (26b)$$

$$\theta = \begin{cases} \arctan \left(\tan \left(k_i \frac{\Omega_i}{2} \right) R_i \right) \div k_i, & \text{if } k_i > 0 \\ \frac{\Omega_i R_i}{2}, & \text{if } k_i = 0 \\ \arcsin \left(\sin \left(k_i \frac{\Omega_i}{2} \right) R_i \right) \div k_i, & \text{if } k_i < 0 \end{cases} \quad (26c)$$

$$\begin{bmatrix} \hat{v}_x \\ \hat{v}_y \\ \hat{v}_z \end{bmatrix} = \left\| \begin{bmatrix} \vec{f}_x \\ \vec{f}_y \\ 1 \end{bmatrix} \begin{bmatrix} \sin(\theta)/R_i \\ \sin(\theta)/R_i \\ \cos \theta \end{bmatrix} \div \begin{bmatrix} 1 \\ l_i(1-s_i) + s_i \\ 1 \end{bmatrix} \right\| \quad (26d)$$

$$R_o = \begin{cases} \tan(k_o \theta) \div \tan \left(k_o \frac{\Omega_o}{2} \right), & \text{if } k_o > 0 \\ \theta \div \frac{\Omega_o}{2}, & \text{if } k_o = 0 \\ \sin(k_o \theta) \div \sin \left(k_o \frac{\Omega_o}{2} \right), & \text{if } k_o < 0 \end{cases} \quad (26e)$$

$$\begin{bmatrix} \vec{f}'_x \\ \vec{f}'_y \end{bmatrix} = \begin{bmatrix} \hat{v}_x \\ \hat{v}_y \end{bmatrix} \frac{R_o}{\sqrt{\hat{v}_x^2 + l_o \hat{v}_y^2}} \begin{bmatrix} 1 \\ l_o(1-s_o) + s_o \end{bmatrix} \quad \blacksquare \quad (26f)$$

Input picture coordinates are represented by $\vec{f} \in \mathbb{R}^2$, while output picture coordinates are denoted as $\vec{f}' \in \mathbb{R}^2$.

2.2 Perspective map algorithms for various projections

Algorithms presented below produce visual sphere vector map in various projections, which can be later used as an input for perspective map rasterizer. Result vector $\hat{v} \in [-1, 1]^3$ can be mapped to picture color range $[0, 1]^3$ by simple transformation:

$$\vec{G}' = \frac{\hat{v} + 1}{2} \quad (27)$$

2.2.1 Rectilinear perspective map

$$\begin{bmatrix} \hat{v}_x \\ \hat{v}_y \\ \hat{v}_z \end{bmatrix} = \begin{cases} \left\| \begin{array}{l} 2\vec{f}_s - 1 \\ (2\vec{f}_t - 1) \div a \\ \cot \frac{\Omega^h}{2} \end{array} \right\|, & \text{if } \Omega \text{ horizontal} \\ \left\| \begin{array}{l} a(2\vec{f}_s - 1) \div \sqrt{a^2 + 1} \\ (2\vec{f}_t - 1) \div \sqrt{a^2 + 1} \\ \cot \frac{\Omega^d}{2} \end{array} \right\|, & \text{if } \Omega \text{ diagonal} \\ \left\| \begin{array}{l} a(2\vec{f}_s - 1) \\ 2\vec{f}_t - 1 \\ \cot \frac{\Omega^v}{2} \end{array} \right\|, & \text{if } \Omega \text{ vertical} \end{cases} \quad (28)$$

Linear perspective map formula, where \hat{v} is the visual sphere vector, \vec{f} represents screen coordinates. a is the screen aspect ratio and Ω the AOV.

2.2.2 Curved panorama map

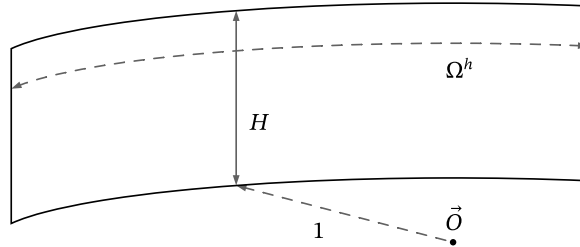


Figure 8: Curved panorama model, where aspect ratio $a = \frac{\Omega^h}{h}$, radius is equal to 1 and \vec{O} denotes arc's origin.

$$a = \frac{\Omega^h}{H} \quad \blacksquare \quad (29a)$$

$$\begin{bmatrix} \vec{f}'_x \\ \vec{f}'_y \end{bmatrix} = \begin{bmatrix} \Omega^h \\ H \end{bmatrix} \left(\begin{bmatrix} \vec{f}_s \\ \vec{f}_t \end{bmatrix} - \frac{1}{2} \right) \quad (29b)$$

$$\begin{bmatrix} \hat{v}_x \\ \hat{v}_y \\ \hat{v}_z \end{bmatrix} = \begin{bmatrix} \sin \vec{f}'_x \\ \vec{f}'_y \\ \cos \vec{f}'_x \end{bmatrix} \quad \blacksquare \quad (29c)$$

Curved panorama perspective-map formula, where a is the panorama aspect ratio, H in the display height-to-radius proportion with Ω^h as the horizontal AOV. Vector \vec{f} represents screen coordinates and \hat{v} is the visual sphere vector.

2.2.3 Full dome map

$$\begin{bmatrix} \vec{f}'_x \\ \vec{f}'_y \end{bmatrix} = \begin{bmatrix} 2\vec{f}_s - 1 \\ 1 - 2\vec{f}_t \end{bmatrix} \quad (30a)$$

$$\theta = |\vec{f}'| \left(\Omega + \frac{\pi}{2} \right) \quad (30b)$$

$$\begin{bmatrix} \hat{v}_x \\ \hat{v}_y \\ \hat{v}_z \end{bmatrix} = \begin{bmatrix} \vec{f}'_x \sin \theta \div |\vec{f}'| \\ \cos \theta \\ \vec{f}'_y \sin \theta \div |\vec{f}'| + o \end{bmatrix} \begin{bmatrix} 1 & 0 & 0 \\ 0 & \cos \varphi & -\sin \varphi \\ 0 & \sin \varphi & \cos \varphi \end{bmatrix} \quad \blacksquare \quad (30c)$$

$$m = \left\{ \frac{1 - |\vec{f}'|}{\partial(1 - |\vec{f}'|)} \right\} \cap [0, 1] \quad \blacksquare \quad (30d)$$

Full dome perspective-map formula, where \vec{f} is the screen coordinates vector. Ω is the compression angle, φ is the tilt angle. \hat{v} represents visual sphere vector. o is the view position offset (in radius) and m is the radial mask with $\partial(x)$ being the equivalent of ***fwidht***(x) function.

2.2.4 Equirectangular projection map

$$\begin{bmatrix} \vec{f}'_x \\ \vec{f}'_y \end{bmatrix} = \pi \begin{bmatrix} 2\vec{f}_s - 1 \\ \vec{f}_t \end{bmatrix} \quad (31a)$$

$$\begin{bmatrix} \hat{v}_x \\ \hat{v}_y \\ \hat{v}_z \end{bmatrix} = \begin{bmatrix} \sin \vec{f}'_x \\ -1 \\ \cos \vec{f}'_x \end{bmatrix} \begin{bmatrix} \sin \vec{f}'_y \\ \cos \vec{f}'_y \\ \sin \vec{f}'_y \end{bmatrix} \quad \blacksquare \quad (31b)$$

Equirectangular projection perspective-map formula, where \vec{f} represents screen coordinates and \hat{v} is the visual sphere vector.

2.2.5 Mirror dome projection map

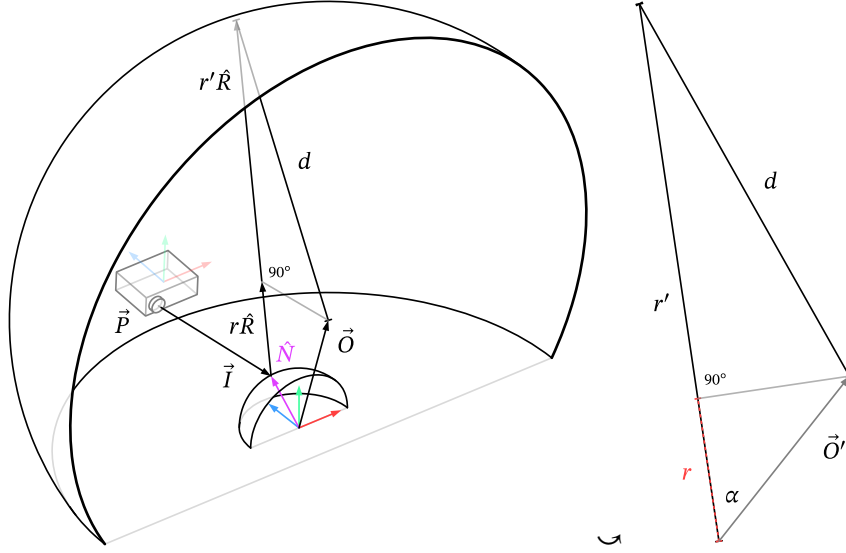


Figure 9: Mirror dome projection model, with mirror center as world origin.⁵

$$\vec{I} = \hat{N} - \vec{P} \quad (32a)$$

$$\hat{R} = \frac{\vec{I} - 2(\vec{I} \cdot \hat{N})\hat{N}}{\|\vec{I} - 2(\vec{I} \cdot \hat{N})\hat{N}\|} \quad (32b)$$

$$\begin{cases} r = \hat{R} \cdot (\vec{O} - \hat{N}) \\ r' = r + \sqrt{d^2 - |r\hat{R} + \hat{N} - \vec{O}|^2} \end{cases} \quad (32c)$$

$$\hat{v} = \frac{r'\hat{R} + \hat{N} - \vec{O}}{d} \quad \blacksquare \quad (32d)$$

$$m = \left(\frac{r' + |\vec{I}|}{(r' + |\vec{I}|)_{\max}} \right)^2 \quad \blacksquare \quad (32e)$$

Mirror dome projection perspective-map formula, where \vec{I} represents incident vector. $\hat{N} \in [-1, 1]^3$ is the spherical-mirror world-normal and surface position, \vec{P} is the projector position, \hat{R} is reflection vector, r' is the reflection distance to dome intersection, as:

$$\hat{R} \cdot (\vec{O} - \hat{N}) = \hat{R} \cdot \vec{O}' = |\hat{R}| |\vec{O}'| \cos \alpha = |\vec{O}'| \frac{r}{|\vec{O}'|} = r \quad (33)$$

$\hat{v} \in [-1, 1]^3$ is the visual sphere vector as mirror surface color and \vec{O} is the dome origin position with d as dome radius. Mirror radius is equal 1 with its origin at position $[0 \ 0 \ 0]$. Light dimming mask is represented by m and it's based

on inverse-square law approximation. In order to produce perspective map image, first mirror 3D model world-normal pass must be produced, as viewed from projector's perspective. It is possible to render the view with additional perspective map of the projector.

Remark. Mirror dome projection system was originally developed by P. BOURKE.⁵

2.2.6 Projection mapping perspective map

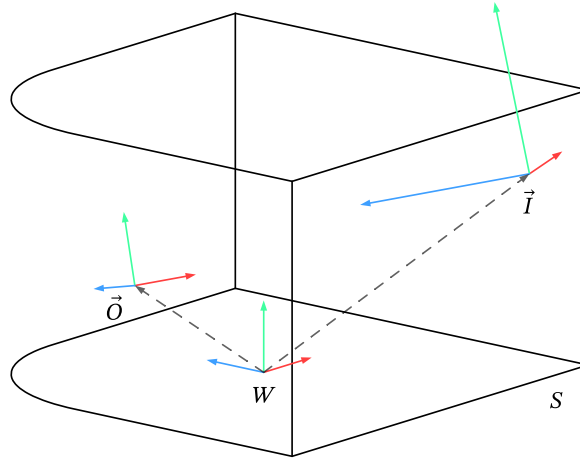


Figure 10: Projection mapping model, with W as the world origin coordinates, \vec{O} as observation point, \vec{I} as projector position and S as projection surface.

$$\begin{bmatrix} \hat{v}_x \\ \hat{v}_y \\ \hat{v}_z \end{bmatrix} = \frac{\begin{bmatrix} \vec{S}_x - \vec{O}_x \\ \vec{S}_y - \vec{O}_y \\ \vec{S}_z - \vec{O}_z \end{bmatrix}}{\|\vec{S} - \vec{O}\|} \begin{bmatrix} W'_{11} & W'_{12} & W'_{13} \\ W'_{21} & W'_{22} & W'_{23} \\ W'_{31} & W'_{32} & W'_{33} \end{bmatrix} \quad \blacksquare \quad (34a)$$

$$m = \left(\frac{|\vec{S} - \vec{I}|}{|\vec{S} - \vec{I}|_{\max}} \right)^2 \quad \blacksquare \quad (34b)$$

Projection mapping perspective-map formula, where \hat{v} represents the visual sphere unit-vector. \vec{S} is the environment surface position, as seen through projector's point of view. \vec{O} denotes observation point. W' is the optional rotation matrix for the world position \vec{S} . Light dimming mask is denoted by m , which value is based on the inverse-square law. \vec{I} represents the projector world position.

In order to produce perspective map image, first 3D model of the projection environment must be produced. Then world position map S must be rendered from projector point-of-view. Position map S changes only if projector position \vec{I} changes, so the map can be reused at each frame even if the observation position is dynamic. For more about projection mapping, see example 1 in sub-subsection 1.1.5 on page 12.

2.2.7 Cube-mapping perspective map

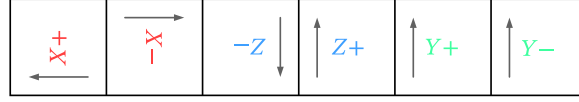


Figure 11: Cube map model with face orientation.

$$\begin{cases} \hat{X} = [1 & 0 & 0]^T \\ \hat{Y} = [0 & 1 & 0]^T \\ \hat{Z} = [0 & 0 & 1]^T \end{cases} \quad (35a)$$

$$i = \lfloor 6\vec{f}_s \rfloor$$

$$\begin{bmatrix} \hat{v}_x \\ \hat{v}_y \\ \hat{v}_z \end{bmatrix} = \begin{bmatrix} (6\vec{f}_s) \bmod 1 - 1/2 \\ \vec{f}_t - 1/2 \\ 1/2 \end{bmatrix} \cdot \begin{cases} [\hat{Z} & -\hat{X} & -\hat{Y}]^T, & \text{if } i = 0 \\ [-\hat{Z} & \hat{X} & -\hat{Y}]^T, & \text{if } i = 1 \\ [\hat{X} & -\hat{Y} & -\hat{Z}]^T, & \text{if } i = 2 \\ [\hat{X} & \hat{Z} & -\hat{Y}]^T, & \text{if } i = 4 \\ [-\hat{X} & -\hat{Z} & -\hat{Y}]^T, & \text{if } i = 5 \end{cases} \quad (35b)$$

Cube-mapping perspective-map formula, where \hat{v} represents visual sphere vector and \vec{f} is the screen coordinate. $[\hat{Z} \ -\hat{X} \ -\hat{Y}]$ represents rotation matrix of each cube side. Operation $x \bmod 1$ is equivalent to **fract**(x) function.

2.2.8 Multiple-screen array map

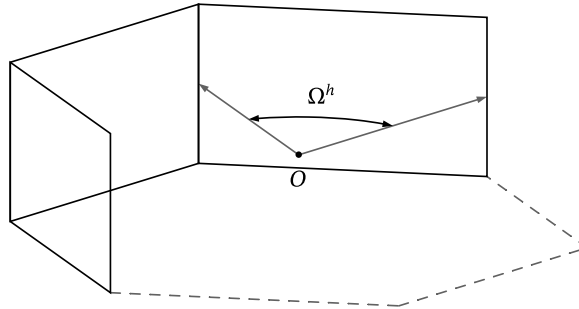


Figure 12: Screen array model with $\Omega^h = 2/6 \pi$, and O as observation point.

$$i = \lfloor n\vec{f}_s \rfloor + \frac{1-n}{2} \quad (36a)$$

$$\begin{bmatrix} \hat{v}_x \\ \hat{v}_y \\ \hat{v}_z \end{bmatrix} = \left\| \begin{bmatrix} 2((n\vec{f}_s) \bmod 1) - 1 \\ (2\vec{f}_t - 1)n \div a \\ \cot \frac{\Omega^h}{2} \end{bmatrix} \right\| \begin{bmatrix} \cos(i\Omega^h) & 0 & \sin(i\Omega^h) \\ 0 & 1 & 0 \\ -\sin(i\Omega^h) & 0 & \cos(i\Omega^h) \end{bmatrix} \quad \blacksquare \quad (36b)$$

n -screen array perspective-map formula, where n is the number of screens, \hat{v} represents visual sphere vector, \vec{f} is the screen coordinates vector, with Ω and a being a single-screen AOV and aspect ratio, respectively.

2.2.9 Virtual Reality perspective map

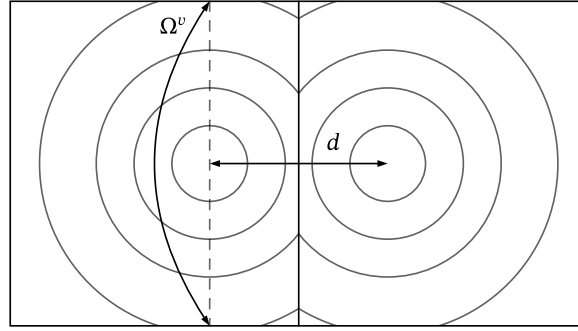


Figure 13: Virtual Reality model with d as the IPD distance relative to total screen width. Such that $d = \frac{\text{IPD}}{\text{width}}$.

$$i = \text{sign}(\vec{f}_s - 1/2) \quad (37a)$$

$$\begin{bmatrix} \vec{f}'_x \\ \vec{f}'_y \end{bmatrix} = \left(\begin{bmatrix} 2((2\vec{f}_s) \bmod 1) - 1 \\ 2\vec{f}_t - 1 \end{bmatrix} + \begin{bmatrix} i(1-2d) \\ 0 \end{bmatrix} \right) \begin{bmatrix} 0.5a \\ 1 \end{bmatrix} \quad (37b)$$

$$\begin{bmatrix} \vec{f}''_x \\ \vec{f}''_y \end{bmatrix} = \begin{bmatrix} \vec{f}'_x \\ \vec{f}'_y \end{bmatrix} \frac{\overbrace{1 + k_1|\vec{f}'|^2 + k_2|\vec{f}'|^4 + \dots + k_n|\vec{f}'|^{2n}}^{\text{radial lens distortion}}}{\underbrace{1 + k_1 + k_2 + \dots + k_n}_{\text{bounds normalization}}} \quad (37c)$$

$$\begin{bmatrix} \hat{v}_x \\ \hat{v}_y \\ \hat{v}_z \end{bmatrix} = \left\| \begin{bmatrix} \vec{f}''_x \\ \vec{f}''_y \\ \cot \frac{\Omega^v}{2} \end{bmatrix} \right\| \quad \blacksquare \quad (37d)$$

Virtual reality perspective map formula, where \vec{f} represents screen coordinates, d is the interpupillary distance (IPD) in screen-width scale, a is the screen aspect ratio, k_1, k_2, \dots, k_n represent lens-distortion coefficients. \hat{v} is the visual sphere vector and Ω^v is the vertical AOV.

Remark. VR perspective map can also be combined side-by-side with a regular perspective map. In extended desktop environment, extra perspective map could provide a monitor preview of the VR content, without an additional render call.

2.3 Lens distortion of perspective picture

Creating perspective picture of a real optical system may require additional deformation of the vector data. Most commonly used algorithm for this purpose is the *Brown-Conrady* lens distortion model.³²

$$r^2 = \vec{f} \cdot \vec{f} \quad (38a)$$

$$\begin{aligned} \begin{bmatrix} \vec{f}'_x \\ \vec{f}'_y \end{bmatrix} &= \begin{bmatrix} \vec{f}_x \\ \vec{f}_y \end{bmatrix} + \overbrace{(k_1 r^2 + k_2 r^4 + \dots + k_n r^{2n})}^{\text{radial distortion}} \begin{bmatrix} \vec{f}_x \\ \vec{f}_y \end{bmatrix} \\ &+ \underbrace{\begin{pmatrix} p_1 \\ p_2 \end{pmatrix} \cdot \begin{bmatrix} \vec{f}_x \\ \vec{f}_y \end{bmatrix}}_{\text{thin prism}} \begin{bmatrix} \vec{f}_x \\ \vec{f}_y \end{bmatrix} + \underbrace{\begin{bmatrix} q_1 r^2 \\ q_2 r^2 \end{bmatrix}}_{\text{decentering}} \end{aligned} \quad \blacksquare \quad (38b)$$

Where r is the dot product of two \vec{f} vectors. k_1, k_2 and k_n are the radial distortion coefficients. q_1 and q_2 are the decentering coefficients. Thin prism distortion coefficients are denoted by p_1 and p_2 .

3 No-parallax point mapping

Real optical systems exhibit phenomenon known as the floating no-parallax point,¹⁸ where each incident vector originates from different position within the lens. Meaning that real optical systems are not complicit with pinhole projection model. In pinhole model all incident vectors share same crossing point. Therefore to simulate optical projection, view position has to change accordingly to incident vector origin of the calibrated lens, or in contrary, visible point should move the opposite way. In spherical lens, NPP offset is in z -direction and can be described as a product of a function $\text{parallax}(\theta)$. As it changes accordingly to an angle between incident vector and the optical axis. Offset value can be approximated by optical measurement of parallax miss-alignment (see figure 21 on page 41).

To calibrate lens distortion with floating NPP, first static NPP picture must be obtained. If camera lens does not produce such image, it can be derived from a sequence of images, each taken at different z position (see subfigure 21d on page 41). In such image composite, every point of the picture plane shares common incident vector origin (in world-space). From this, two lens maps can

be derived, *parallax offset map* from sequence's pixel z position and *perspective map* from composite image of calibration rig/chart.

To render picture with floating NPP, each 3D point must be transformed prior to rasterization. Transformation is done accordingly to the perspective map incident position and associated parallax offset value. Either by moving the point or the view position. Noticeably the parallax offset value can also be encoded in a graph (for simple spherical lenses), instead of a texture map.

Rendering with rasterization would produce approximate result as values in-between vertices are interpolated, not transformed. Therefore best quality floating-NPP result is to be expected from ray-tracing. In such case, offset of a ray-origin-position should be performed. An equivalent of visual-sphere offset (see subfigure 21b on page 41). Going back to rasterization, point offset can be achieved through projection of the *parallax offset* texture map onto the scene geometry. Each geometry point can be transformed in view-space z direction by a value from projected *parallax offset* texture.

4 Appendix

Perspective picture visible inside the visual space gives some sense of immersion (e.g. picture, film, computer game) even without visual illusion.⁹ That's because it is perceived as a visual symbol of an abstract point of view, through which not picture plane is seen, but depicted space's mind-reconstruction. The picture immersion does not break, as long as appearance of the objects do not exhibit too much deformation. Perceiving abstract point of view invokes separation from the surrounding. To enhance immersion, environment stimuli is being reduced. In a movie theater, to uphold the immersion lights are turned off and silence is expected. Horror-gameplay session are usually played at night, to separate from safe-space of home. This approach focuses virtual presence on depicted space.

Remark. On the opposite side, picture as an integral part of the surrounding can be categorized under the *Trompe-l'œil* technique.³¹

Through the perception of the picture, physical properties of depicted space and objects within it are estimated. Mind fills the gaps, as symbols are always simplified versions of the real thing.

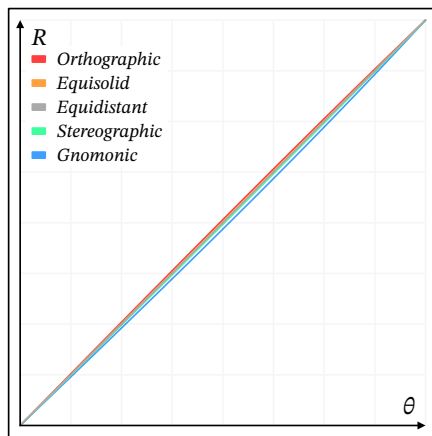
Example. Cup of coffee laying on a table has only one side visible at once, but it can be assumed that the opposite one is there too, since shape of the cup is known. This is a blank information filled by the mind.

Physical objects have their physical properties, but their visual symbols have some physical properties too, like angular size, perspective, shadow, etc. Those visual properties give some information about physical. In case of perspective, visual properties give information about depicted space and about point of view. Since most of the time picture represents a point of view (e.g. film, video game, visualization), it is wise to consider subject's properties of vision when

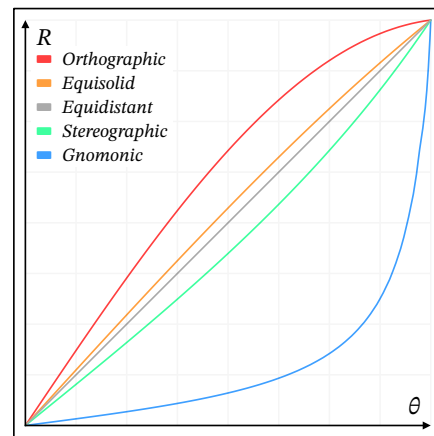
designing picture perspective. But instead of producing mechanical simulation, perspective should symbolize total sensory experience.²

Theorem 1. *To create immersive visual symbol of a visual space, it is necessary to use curvilinear perspective instead of a linear.*

Proof. Geometry of human visual space contradicts linear perspective principle, as visual field extends beyond linear perspective angle of view. Linear perspective, based on a tangent of an angle, exhibits limit of $179.(9)8^\circ$ of view. While visual field extends horizontally up to 220° for binocular vision.¹⁶ ■



(a) Graph plotting ray of angle $\theta \in [0^\circ, \Omega]$ — as the horizontal axis, and screen-position radius $R \in [0, 1]$, as the vertical axis, where $\Omega = 40^\circ$ which is equivalent to $R = 1$.



(b) Graph plotting ray of angle $\theta \in [0^\circ, \Omega]$ — as the horizontal axis, and screen-position radius $R \in [0, 1]$, as the vertical axis, where $\Omega = 170^\circ$ which is equivalent to $R = 1$.

Figure 14: Chart comparison of radial compression in five major azimuthal projections, across two different AOV (Ω) values: narrow (14a) and wide (14b).

At narrow AOV both types of perspective are suitable for immersive picture. In such case differences between each projection are negligible. Subfigure 14a presents those differences in comparison to five major perspective projections. Same differences seem exaggerated at higher AOV values (see subfigure 14b).

Corollary 1.1. *Practical limit for immersive picture in linear perspective is between 60° and 110° AOV. Wider-angles exhibit deformations known as the Leonardo Paradox,⁹ which are then dominant in the image perception and break picture's immersion.* ■

To show wider-angle picture it is necessary to use curvilinear projection. But there is a tendency to see the world not through sight but understanding. We understand that the wall is flat, therefore we see it that way. Picture projected

into the eye is just a visual symbol and has its own physical properties (e.g. perspective and shape). Therefore its visual representation is curvilinear, where the curvature symbolizes wider field of view. Reader can validate curvilinear nature of human visual space,^{4,12} by following A. RADLEY experiment²⁵:

“Also when you have a moment, get a 30 cm ruler (...), and whilst looking forward bring it close to the bottom of your nose, and notice how its shape at the outer edges curves upwards and forwards. It may take you a few minutes to be able to see this effect, because you are so accustomed to not noticing it ! But once you do you will be amazed to see your curved field of view as it really is for the first time.” — A. RADLEY

4.1 Visual space symbolic picture

Since we came into conclusion that symbol of a visual space is curvilinear, there is a task of selecting between many non-linear projections. Each has properties that symbolize subject’s perception or information span about depicted space. Not appearance of the symbol should dominate the picture, but projected information about point of view and depicted space properties.

Problem 1. Which curvilinear perspective is best for visual symbol of visual space?

Proposition 1.1. A model based on anamorphic lens geometry; a mix between fish-eye, panini and anamorphic projection.

fish-eye as it can represent wider AOV than linear perspective (e.g. π) and conforms to the curvilinear nature of VS. Gives natural spatial awareness.

panini to symbolize binocular vision; two spherical projections combined into one panoramic image.^a Produces picture geometry more familiar to the viewer.

anamorphic as cylindrical projection, like *Panini*, tends to elongate proportions vertically; there is a need for correction. Correction should make object in focus proportional as it varies depending on position and size.

Remark. Only linear anamorphic correction will conform to the perspective picture definition (see on page 35).

Remark. Equations in subsection 2.1 on page 16 (about perspective transformation) presents variables that drive all mentioned above geometrical factors.

^aEffect is also referred to as *Stereopsis*.

4.2 Visual sphere as a whole image

Common idea of an image is limited to a finite 2-dimensional plane. Which is subjective, due to constraints of human visual field and up-front placement of eyes. One can construct a rectangular frame, which at certain distance from the eyes will cover full visual field (VF). In case of some animals (e.g. horse, rabbit), visual space confines much wider VF. With only few blind spots, spanning to almost 360° AOV.^{3,19} Such field cannot be enclosed by a single rectangular frame. Thus image nature is not of a frame. Another model has to be chosen instead. One able to cover full $\Omega = 360^\circ$ is a sphere.

Remark. Cylindrical projection cannot cover full 360° AOV in all directions. It is a hybrid between frame and spherical model. When vertically-oriented, full $\Omega^v < 180^\circ$.

All three-dimensional space around given observation point, can be projected onto a sphere, with given observation point as a origin. Even the sphere itself is a 3D object, its surface (as well as image nature)²⁶ is two-dimensional. Therefore creating perspective picture is a matter of representing portion of the visual sphere on a flat surface; a fundamental topic in cartography. Concept of a sphere as a model of visual space goes back as far as 300 BC, where Greek mathematician EUCLID seem first to mention (others are L. DA VINCI and F. AGUILONIUS).³⁰

Remark. Each projection of sphere onto a flat surface is a compromise and can preserve only some properties (e.g. shape, area, distance or direction), which in case of perspective picture relates to some symbolic information about physical space.

Definition 1. Let us define perspective picture as the azimuthal projection, where lines converging at optical axis vanishing point remain straight, that *conservation of perspective* may occur (see definition on page 35).

4.2.1 Physical space properties preserved in azimuthal projections

Below are presented static properties of five major azimuthal projections. Properties of motion can be found in sub-subsection 4.3.2 on page 33. It is important to know which symbolic information about space is carried in each perspective projection, so that design choice for perspective geometry may be conscious.

Gnomonic (rectilinear) projects all great circles as straight lines, thus preserving directions. For 3D projection, straight lines in object-space remain straight. It does not preserve proportions, angles nor area or distances (see subfigure 15a on page 32). Extreme distortion occurs away from the center, in a form of radial stretch (see *Leonardo Paradox*)⁹. AOV $\Omega \in (0, \pi)$.

Example. Most common perspective type in painting, 3D graphics and architectural visualization. Sometimes it is used to overemphasize building appearance by leveraging *Leonardo Paradox*.⁹ Wide AOV combined with

lowered optical center creates an effect of acute corners. This produces an extraordinary look. Such visual-trick may confuse the public, as experience of symbolic picture won't match building visual-space appearance.

Stereographic (conformal) preserves angles (at line intersection point). There is no perceivable radial compression, thus smaller figures retain their shape. It does not preserve distances (non-isometric), nor angular surface area. For 3D projection, most important factor is the conservation of proportions (see subfigure 15b on the following page). AOV $\Omega \in (0, 2\pi)$.

Example. In a picture with stereographic projection, face of the actor keeps its shape and proportions, even at wide AOV. This projection also gives best spatial-awareness sensation (where visual cues are available). Good use case is navigation through tight spaces and obstacles.

Equidistant preserves angular distance from the center point (see subfigure 15c on the next page). For 3D projection, angular speed of motion is preserved. Radial compression remains low-to-moderate at extreme Ω angles. AOV $\Omega \in (0, 2\pi]$.

Example. This projection is recommended for target aiming or radar map navigation, where all targets are projected onto a Gaussian Sphere.

Equisolid preserves angular area. Gives good sensation of distance (see subfigure 15d on the following page). Radial compression is moderate up to π . Near maximum Ω , compression is high. AOV $\Omega \in (0, 2\pi]$.

Example. When there are no spatial cues, this is best projection for putting emphasis on the distance to the viewer.¹⁵ Good use case is flight simulation, where only sky and other aircraft are in-view.

Orthographic preserves brightness. It is a parallel projection of a visual hemisphere. Has extreme radial compression, especially near π (see subfigure 15e on the next page). AOV $\Omega \in (0, \pi]$.

Example. Most commonly found in very cheap lenses, like the peephole door viewer. Thanks to brightness being proportional to occupied image area, it found common use in sky photography and scientific research.^{21,28}

4.3 Image geometry and sensation of motion

Picture perspective affects the way motion is perceived. It can enhance certain features, like proportions and shapes, movement or spatial-awareness. It can also guide viewer attention to a specific region of image (e.g. center or periphery). Knowledge about those properties is essential for conscious image design.

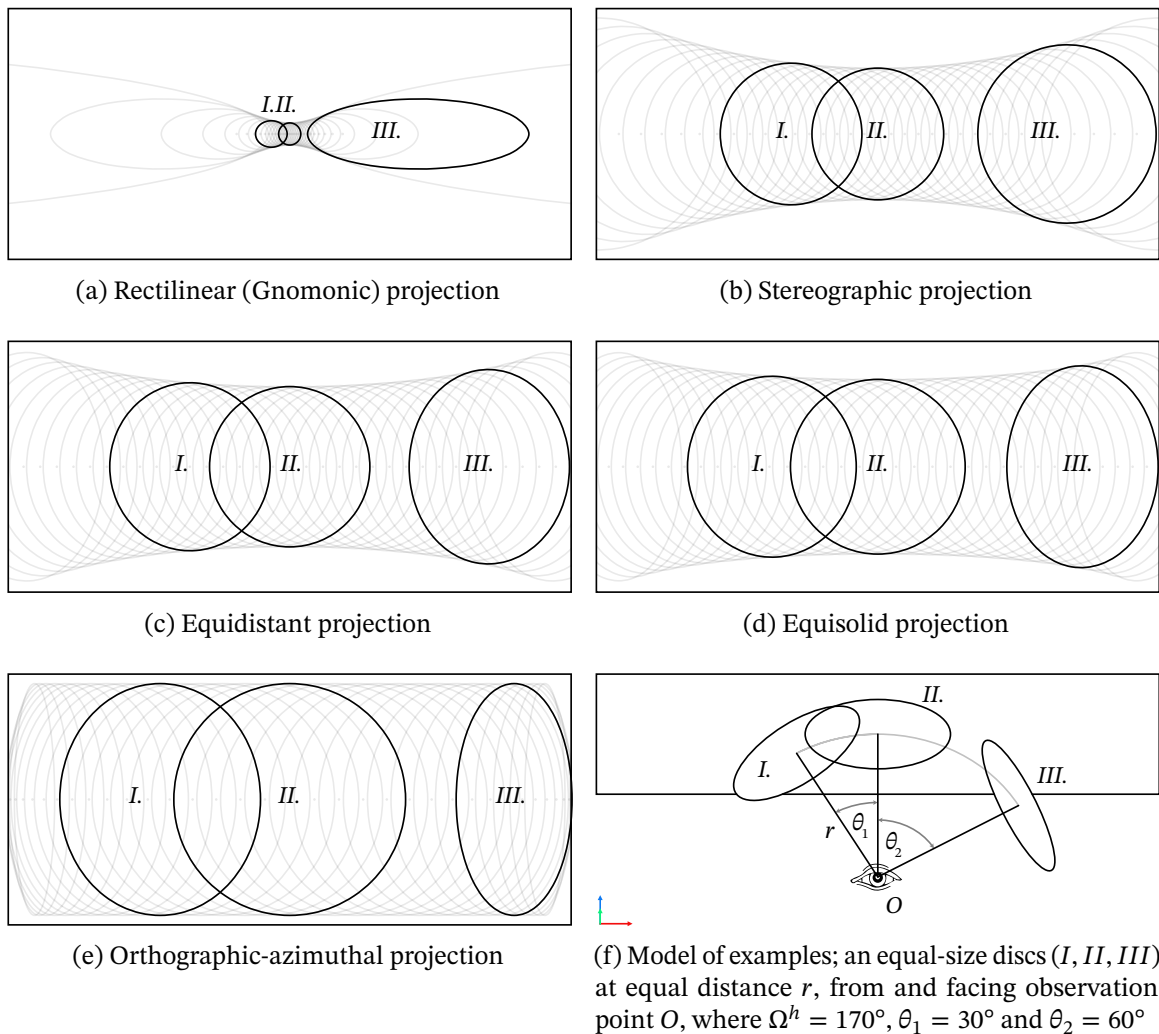


Figure 15: Example of motion in perspective picture of various azimuthal projections. Here subfigure 15f presents viewed elements layout.

4.3.1 Attention focusing

In film design, there are several techniques that focus viewer attention on a specific portion of the picture (like *motion*, *color*, *light* and *composition*). Attention focusing through composition and motion is related to picture's perspective, as its geometry can compress and stretch the image. In composition, *rule of thirds* states that viewer attention focuses on four corners of a rectangle produced by division of an image into three, equally-sized rows and columns. In motion, attention generally drives toward objects approaching the camera or those growing in scale. Attention also focuses on objects entering image frame. Same rules apply loosely in reverse, as attention suspense. Filmmakers tend to

frame the image so that region of interest lays in accordance to the *rule of thirds*. In case of computer games, region of interest is usually located at the very center, thus viewer must overcome the *principle of thirds* and some properties of *linear perspective* in order to switch attention to that region. In order to focus on the center, games usually incorporate some non-diegetic elements, like crosshair. Such approach may lower immersiveness of symbolic picture.⁶

4.3.2 Attention focusing motion in perspective

Radial stretching and compression are the main attention focusing factors of perspective projection. They give subconscious sensation of movement towards camera, and can amplify figure screen-relative speed of motion.

Gnomonic (rectilinear), due to extreme radial stretch attention drives towards periphery. When approaching image bounds figure grows in scale and speed (see subfigure 15a on the preceding page). This combined with motion-sensitive peripheral vision adds to the effect. At wider AOV amplified motion breaks immersion of symbolic picture.

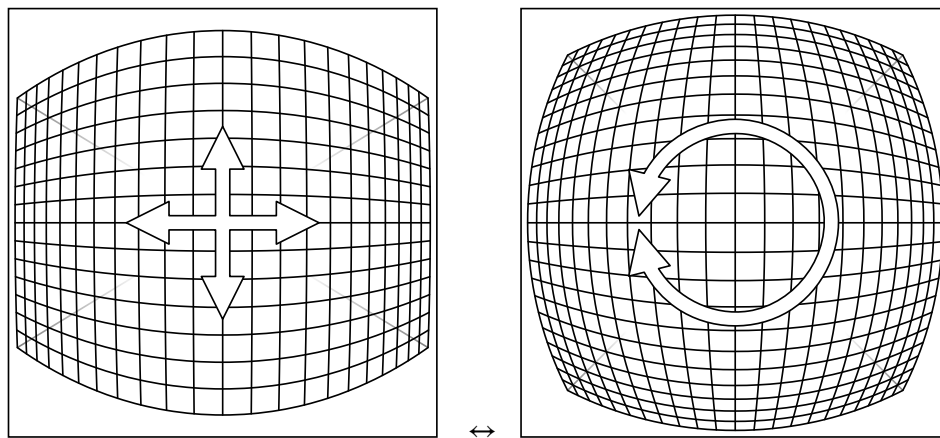
Stereographic also draws attention towards periphery. Figures grow in scale near bounds, but immersion does not break, as proportions are preserved, even at wide AOV (see subfigure 15b on the previous page).

Equidistant drives attention toward center, as figures in periphery are radially compressed (see subfigure 15c on the preceding page). This projection preserves screen-relative, radial speed of motion, making it uniform and representative across the picture.

Equisolid also drives attention toward the center, as radial compression is even greater (see subfigure 15d on the previous page). Figure speed of motion in screen-space slightly declines towards periphery.

Orthographic has extreme radial compression that breaks immersion of a symbolic picture (see subfigure 15e on the preceding page). When in motion, image seem to be imposed on an artificial sphere.

Gnomonic and *Orthographic* projections are the two extremes of azimuthal spectrum. They both are least suited for an immersive picture. *Cylindrical* perspective type, while symbolizing binocular vision, also gives visual cue for the vertical axis orientation. Such cue is undesirable in case of camera roll-motion, or when view is pointing up/down, as image vertical axis will then not be aligned with depicted space orientation. In such case perspective geometry should transition to *spherical* projection (see figure 16 on the next page).



(a) Example of image geometry for pitch/yaw motion (arrows), where $\Omega^h = 120^\circ$, $k = 0$, $l = 10\%$ and $s = 95\%$.

(b) Example of image geometry for roll motion (arrows), where $\Omega^h = 120^\circ$, $k = 0$, $l = 100\%$ and $s = 95\%$.

Figure 16: Examples of image geometry for a given view-motion type.

4.4 History of the topic and previous work

Current image abstract theorem was established in 15th century book *De Pictura*, by L. B. ALBERTI. Based on invention of F. BRUNELLESCHI, ALBERTI defined geometrical and theoretical rules for perspective projection design.² These rules are currently used in polygon-based CG graphics. Major theoretical statement that laid foundation on image projection technology and present understanding of image nature can be traced back to ALBERTI abstract definition of image. He described painting being like a window in a wall¹:

“First of all, on the surface on which I am going to paint, I draw a rectangle of whatever size I want, which I regard as an open window through which the subject to be painted is seen.” — L. B. ALBERTI

But in times of its discovery, as for now, linear perspective introduced itself with several issues. When there’s a need for a wide-angle view, one close to human visual field, geometrical distortions appear to dominate visual aspect of the picture. These issues were noticed by Renaissance artists, like L. DA VINCI. He put to test the Alberti Theorem and produced paintings of accurate-perspective.⁷ In his *Treatise on Painting*, DA VINCI notes that picture conforms to the idea of a window only when viewed from one specific point in space.⁸ Stating that seen otherwise, objects appear distorted, especially in the periphery. Picture then, viewed from a different point ceases to be like a window in a wall and becomes a visual symbol of an abstract point of view.^b Some 18th century late Baroque and

^bEffect also referred to *Zeeman Paradox*.⁹

Neoclassical artists, when encountered mentioned issues, introduced derivative projections. Like G. P. PANNINI with later re-discovered *Panini Projection*,²³ or R. BARKER, who established the term *Panorama*.³³ This was a new type of perspective. In a form of cylindrical projection, where abstract window frame becomes horizontally curved, reducing deformation artifacts in wide, panoramic depictions of architecture.



Figure 17: Still from TODD-AO HIGH-SPEED ANAMORPHIC lens (35mm T1.4) with visible curvilinear perspective. This type of lens was featured in films like *Conan the Barbarian*, *Dune* and *Mad Max*.²⁹ © 2017 ShareGrid, Inc.

Invention of motion picture followed by the rise of film industry, resulted in a demand for new image geometry. Previously still, now pictures had to be pleasing to the eye, in motion. 1950s brought anamorphic cinematography to the wider audience. Lenses like CINEMASCOPE and later PANAVISION¹⁷ became a standard in film production. Figure 17 shows example of mixed spherical and cylindrical projection with perspective preservation, of anamorphic lens.

Definition 2. *Conservation of perspective* - lines converging at the optical-axis vanishing-point remain straight.

Remark. See also perspective picture definition on page 30.

CG image technology did not follow film industry in that field. Still based on ALBERTI theorem, computer graphics became incompatible with film, generating great costs, when two had to be joined together.²⁷ Stitching such picture requires lens aberration rotoscoping, where geometry correction is performed manually at each frame. Currently in computer-games industry, CG imagery is practically unable to produce realistic, curvilinear simulation of visual space (VS), or even simulate anamorphic lens geometry, due to limits of linear perspective and resource costs of overcoming those issues. Some hybrid solutions were proposed,^{14,15} that combine rasterization with ray-tracing, or tessellation. Such approach allows for a semi-practical and limited production of real-time pictures in a non-linear perspective.

5 Conclusion and future work

Visual sphere perspective model expands possibilities for image creation. Like a vision of a classical artist is richer and more dynamic than his final creation, so should be a model describing image. So much that virtual vision would have to be reduced to fit the medium, with a room for adjustment.

In medieval times people were fascinated with mirror, it depicted reality as it really is, a task impossible for human hand. But mirror could not reflect the vision of imagination, so much as painting. It did not produce realistic reflection of reality, nor reflection of imagination. In art there was a pursuit involving philosophy and religion to reach some imaginary reflection. Only after BRUNELLESCHI experiment proved that painting created by human hand, with strict rules of geometry, reflected from a mirror fits well into reality, artists started pursuing mathematics of art. Film and photography became a new mirror, but still not one of imagination. Finally computer graphics became a format capable to reflect one's vision of imagination, but it struggled to be photo-real.

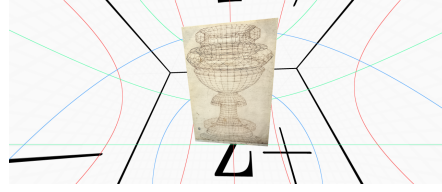
Language of image is ultimately a language of symbols, it works in conjunction with mind, which recreates visual space of the picture. Computer game image is special in a sense, that rather being a viewing glass (like in a film) it impersonates point of view of the protagonist, which invokes different symbolic measures. Real-time graphics should be capable to incorporate such visual symbols. One way for achieve this is to change current perspective model for a bigger one. Proposed here change includes the use of universal perspective model which defines simple variables for manipulation of perspective geometry. It also includes production technique for a real-time imagery using this model. Such new solution fits well into current graphics pipeline, replacing only low-level rasterization processes. Aliasing-free end result is comparable in quality to 8×MSAA and enables previously impossible visual effects in real-time graphics. Presented visual sphere model unites all types of perspective projections under one technical solution, making perspective a fluid construct. Perspective vector-maps can be easily combined and transformed by spherical interpolation. Picture geometry can now be designed to smoothly adapt to the visual story, giving new dimension of control over mental perception of image. Presented concepts and equations may also find their use in other fields, not rendering-related. This is a great base as well as complete solution upon which many new technologies and works can emerge. Some specific use cases still require additional research, like hidden surface removal and no-parallax point mapping. Further studies will include research over calibration and simulation of real optical systems with floating NPP. Also performance tests, comparison to current solutions should be evaluated by future research. Psychological analysis of perspective geometry magnitude of influence on depicted space perception, performed on a large sample data, could be an interesting field to study.

Acknowledgments

Special thanks to ZBIGNIEW RYBCZYŃSKI who told that we don't see the world in rectilinear perspective and that CG image does not match camera lens projection (during his 2010 conference in Cieszyn). This single presentation became a spark for this research. Additional thanks to SHAUN WILLIAMS who combined cylindrical and spherical projection based on a view angle. To ALAN RADLEY and KIM VELTMAN for their interest in this topic and paper. To ARASH SHIVA who provided permission for use of the anamorphic lens test. Final thanks to DOBIEŚŁAW KACZMAREK who taught principles of perspective drawing. And to all unmentioned individuals who gave much needed feedback, it helped greatly improving this paper.



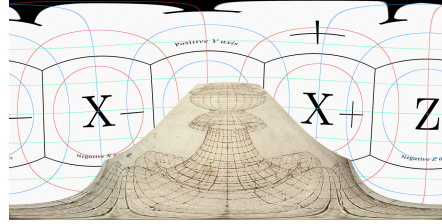
(a) *Vector map* of rectilinear perspective, where $\Omega^d = 140^\circ$, $k = 1$, $l = 1$.



(b) *Rasterized quad* in rectilinear perspective, where $\Omega^d = 140^\circ$, $k = 1$, $l = 1$.



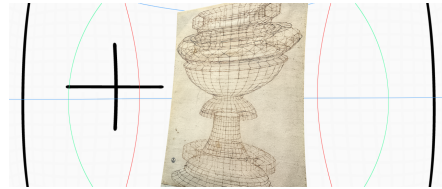
(c) *Equiangular projection vector map* of a whole sphere, where $\Omega^h = 360^\circ$ and $\Omega^v = 180^\circ$.



(d) *Rasterized quad* in equiangular projection, where $\Omega^h = 360^\circ$ and $\Omega^v = 180^\circ$.



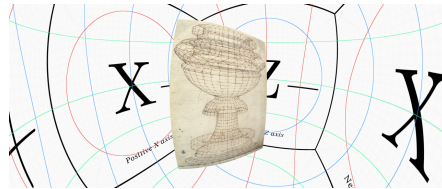
(e) *Vector map* of mustache-type lens distortion, where $\Omega^d = 131^\circ$, $k = 0.32$, $l = 62\%$, $s = 86\%$, $k_1 = -0.6$, $k_2 = 0.4$.



(f) *Rasterized quad* in mustache-type lens distortion, where $\Omega^d = 131^\circ$, $k = 0.32$, $l = 62\%$, $s = 86\%$, $k_1 = -0.6$, $k_2 = 0.4$.



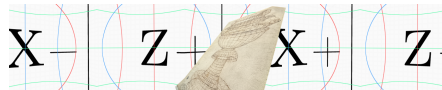
(g) *Vector map* of curvilinear fish-eye perspective, where $\Omega^d = 270^\circ$, $k = 0.32$, $l = 62\%$, $s = 86\%$.



(h) *Rasterized quad* in curvilinear fish-eye perspective, where $\Omega^d = 270^\circ$, $k = 0.32$, $l = 62\%$, $s = 86\%$.



(i) *Vector map* of five-screen horizontal array in rectilinear projection, where single screen $\Omega^{h,v} = 60^\circ$, $k = 1$ and $l = 1$, giving a total $5\Omega^h = 300^\circ$.



(j) *Rasterized quad* in five-screen horizontal array, where single screen $\Omega^{h,v} = 60^\circ$, $k = 1$ and $l = 1$, giving a total $5\Omega^h = 300^\circ$.

Figure 18: Examples of polygon quad rasterization directly from three-dimensional space to image, using visual-sphere vector map G , where $G_{st} \in [0, 1]^3 \leftrightarrow [-1, 1]^3$.

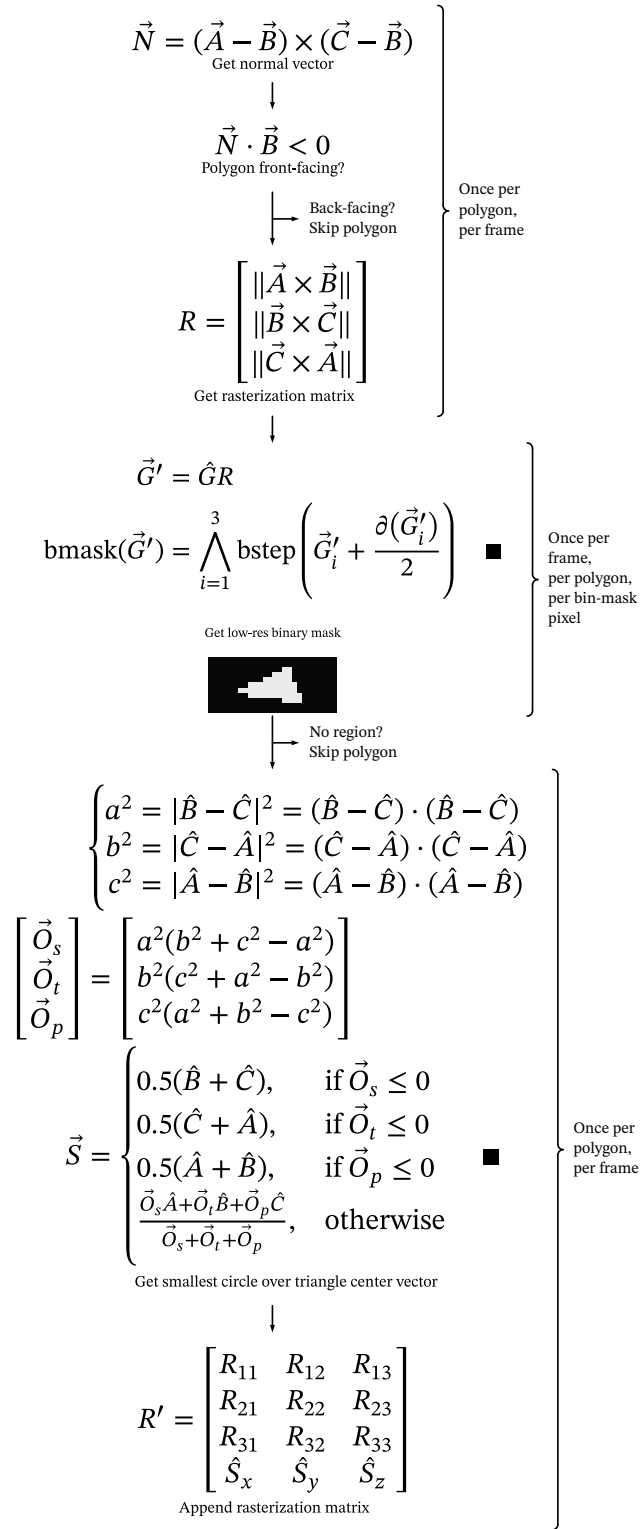


Figure 19: Vertex rasterization process flowchart. Chart starts with $\vec{A}, \vec{B}, \vec{C}$ triangle points (transformed to camera-space) and produces low-resolution binary mask (using perspective vector map G) and 4×3 rasterization matrix R' .

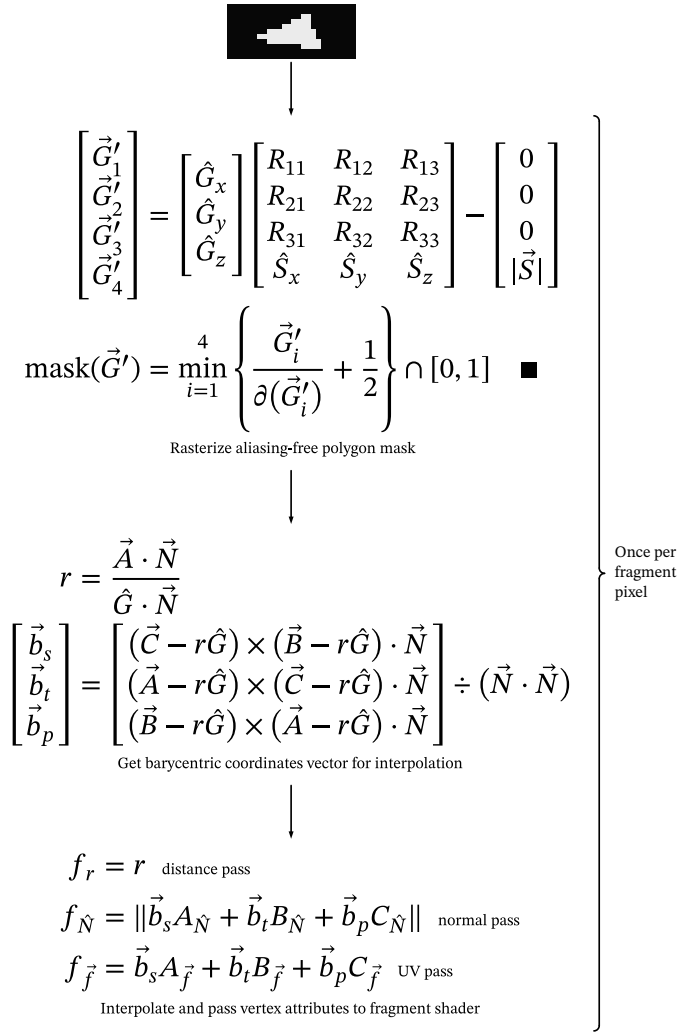
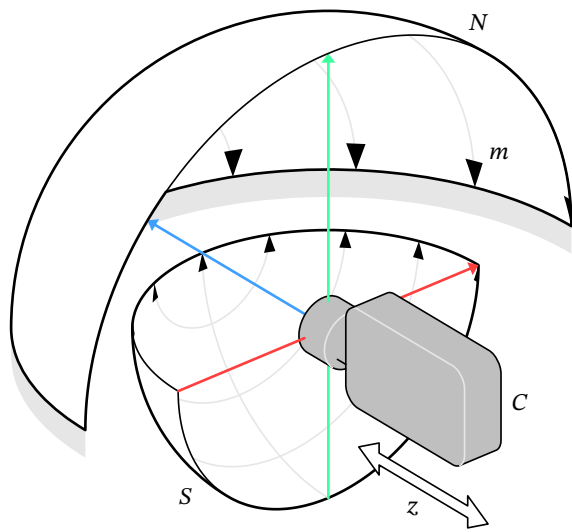
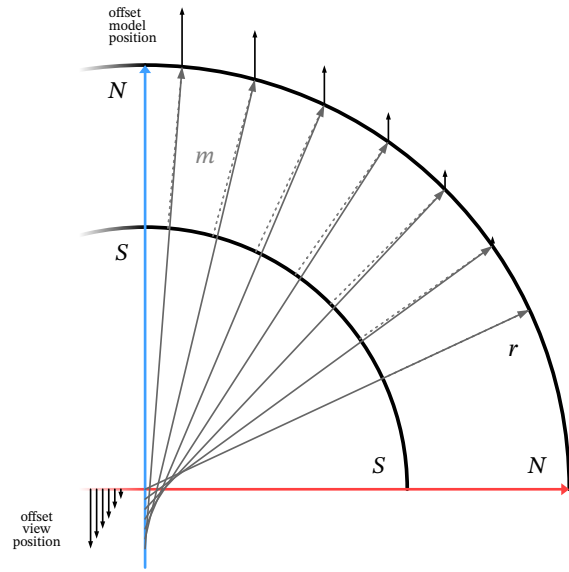


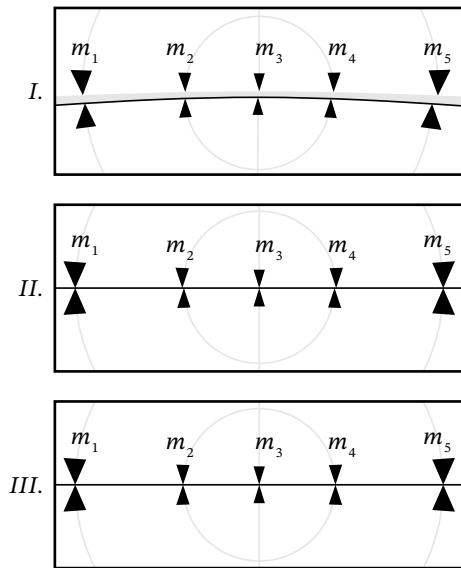
Figure 20: Fragment rasterization process flowchart. Chart starts with rasterization matrix R' , binary mask of render regions, polygon normal vector \vec{N} , triangle points $\vec{A}, \vec{B}, \vec{C}$ and perspective vector map G . For each pixel, aliasing-free mask is produced and barycentric coordinates \vec{b} are calculated, then interpolated vertex data f is passed to fragment shader as output.



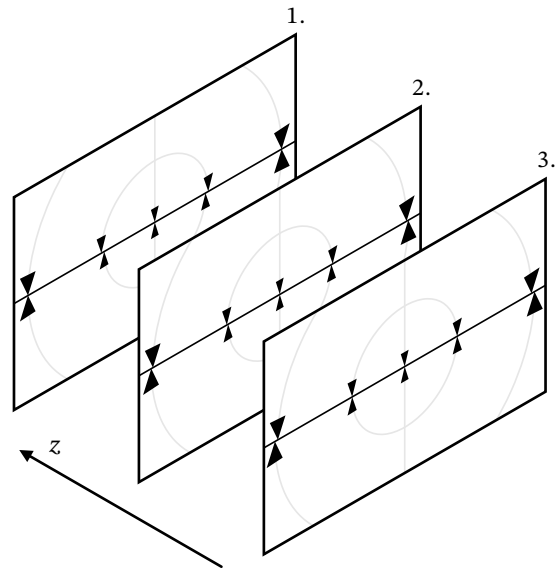
(a) Model of no-parallax point (NPP) calibration rig. Which measures misalignment of m markers between northern (N) and southern hemisphere (S), as seen through camera C .



(b) Simulation of floating NPP in fish-eye camera. Black arrows represent position offset of the model for rasterization and view position offset for ray-tracing. When measuring the NPP (sub-figure 21c), camera travel is opposite to view position offset.



(c) Example *I* presents misalignment of the camera in all three axes. Example *II* presents alignment in X, Y axis, where peripheral marker pair m_1, m_5 are aligned near horizontal AOV, while pairs m_2, m_4 are misaligned due to floating NPP. Example *III* presents "slit-scan" composite of variable z position, where all markers are aligned.



(d) Example of a variable camera position z encoded in an image sequence (1, 2, 3). Element 1 presents alignment of the peripheral markers, while element 3, alignment of the side markers. Element number 2 presents position in-between.

Figure 21: Floating no-parallax point rendering and measurement process.

References

1. Alberti, L. B. in. *On painting and on sculpture* trans. by Grayson, C., 55 (Phaidon, London, England, 1972). http://as.vanderbilt.edu/koepnick/Modernism_f05/materials/images/alberti_window.htm (cit. on pp. 6, 34).
2. Argan, G. C. & Robb, N. A. The Architecture of Brunelleschi and the Origins of Perspective Theory in the Fifteenth Century. *Journal of the Warburg and Courtauld Institutes* **9**, 96. doi:10.2307/750311 (1946) (cit. on pp. 28, 34).
3. Bagley, L. H. & Lavach, D. in Varga, M. *Textbook of Rabbit Medicine E-Book* chap. 9.1 Ocular anatomy and physiology (Butterworth-Heinemann, 2013) (cit. on p. 30).
4. Baldwin, J., Burleigh, A. & Pepperell, R. Comparing Artistic and Geometrical Perspective Depictions of Space in the Visual Field. *i-Perception* **5**, 536–547. doi:10.1068/i0668. <http://journals.sagepub.com/doi/pdf/10.1068/i0668> (2014) (cit. on p. 29).
5. Bourke, P. Low Cost Projection Environment for Immersive Gaming. *Journal of MultiMedia* **3**, 41–46. doi:10.4304/jmm.3.1.41-46. <http://paulbourke.net/papers/dime2006/dime2006.pdf> (2008) (cit. on pp. 22, 23).
6. Casamassina, M. *King Kong's Immersive Style* IGN. <http://ign.com/articles/2005/07/18/king-kongs-immersive-style> (2019) (cit. on p. 33).
7. Da Vinci, L. *Annunciation* oil and tempera on panel. Painting. Uffizi Gallery, Florence, Italy, 1475-1480. http://en.wikipedia.org/wiki/De_pictura#/media/File:Leonardo_Da_Vinci_-_Annunciazione.jpeg (cit. on p. 34).
8. Da Vinci, L. in *A treatise on painting* trans. by Rigaud, J. F., 52 (Project Gutenberg, Salt Lake City, USA, 2014). <http://gutenberg.org/ebooks/46915> (cit. on p. 34).
9. Dixon, R. in *Mathographics* 82–83 (Dover Publications, Great Britain, 1987) (cit. on pp. 27, 28, 30, 34).
10. Dupuy, J. Concurrent Binary Trees (with application to longest edge bisection). *Proceedings of the ACM on Computer Graphics and Interactive Techniques* **3**. doi:10.1145/3406186. <https://hal.archives-ouvertes.fr/hal-02898121/document> (2020) (cit. on p. 15).
11. Ericson, C. *Minimum bounding circle (sphere) for a triangle (tetrahedron)* <http://realtimecollisiondetection.net/blog/?p=20> (2020) (cit. on p. 9).

12. Erkelens, C. J. The Perspective Structure of Visual Space. *i-Perception* **6**. doi:10.1177/2041669515613672. <http://journals.sagepub.com/doi/pdf/10.1177/2041669515613672> (2015) (cit. on p. 29).
13. Fuchs, H., Kedem, Z. M. & Naylor, B. F. *On visible surface generation by a priori tree structures* in *Proceedings of the 7th annual conference on Computer graphics and interactive techniques - SIGGRAPH 80* (ACM Press, 1980). doi:10.1145/800250.807481 (cit. on p. 15).
14. Gascuel, J.-D., Holzschuch, N., Fournier, G. & Péroche, B. *Fast Non-linear Projections Using Graphics Hardware* in *ACM Symposium on Interactive 3D Graphics and Games* (ACM, Redwood City, California, 2008), 107–114. doi:10.1145/1342250.1342267. <http://maverick.inria.fr/Publications/2008/GHFP08/i3d2007.pdf> (cit. on p. 35).
15. Glaeser, G. & Gröller, E. Fast generation of curved perspectives for ultra-wide-angle lenses in VR applications. *The Visual Computer* **15**, 365–376. doi:10.1007/s003710050185 (1999) (cit. on pp. 31, 35).
16. Hueck, A. *Von den Grenzen des Sehvermögens* ger, 84. http://hans-strasburger.userweb.mwn.de/materials/hueck_1840_ocr.pdf (Müller's Archiv, Tartu, 1840) (cit. on p. 28).
17. Königsberg, I. *The complete film dictionary* 12. <http://archive.org/details/completfilmdict00koni> (Nal Penguin INC, New York, USA, 1987) (cit. on p. 35).
18. Littlefield, R. Theory of the No-Parallax Point in Panorama Photography. <http://janrik.net/PanoPostings/NoParallaxPoint/TheoryOfTheNoParallaxPoint.pdf> (2006) (cit. on p. 26).
19. Miller, P. E. & Murphy, C. J. in *Equine Ophthalmology* (ed Gilger, B. C.) chap. Visual perspective and field of view (Elsevier Health Sciences, St. Louis, USA, 2010) (cit. on p. 30).
20. Muszyński, G., Guzek, K. & Napieralski, P. *Wide Field of View Projection Using Rasterization* in *Multimedia and Network Information Systems* (eds Choroś, K., Kopel, M., Kukla, E. & Siemiński, A.) (Springer International Publishing, Cham, 2019), 586–595. doi:10.1007/978-3-319-98678-4_58 (cit. on p. 2).
21. *NIKKOR - The Thousand and One Nights* No.6. Nikon Corp. <https://imaging.nikon.com/history/story/0006/index.htm> (cit. on p. 31).
22. Newell, M. E., Newell, R. G. & Sancha, T. L. *A solution to the hidden surface problem* in *Proceedings of the ACM annual conference on - ACM72* (ACM Press, 1972). doi:10.1145/800193.569954 (cit. on p. 15).
23. Pannini, G. P. *Interior of St. Peter's* oil on canvas. Painting. National Gallery of Art, Washington DC, USA, 1754. <http://web.archive.org/web/20130327080328/vedutismo.net/Pannini/> (cit. on p. 35).

24. Pineda, J. A parallel algorithm for polygon rasterization. *ACM SIGGRAPH Computer Graphics* **22**, 17–20. doi:10.1145/378456.378457. <https://doi.org/10.1145/2F378456.378457> (1988) (cit. on p. 7).
25. Radley, A. in Cipolla-Ficarra, F. V. *Handbook of Research on Interactive Information Quality in Expanding Social Network Communications* 46 (IGI Global, 2015). <http://books.google.com/books?id=90yfbWAAQBAJ> (cit. on p. 29).
26. Rybczyński, Z. *a Treatise on the Visual Image* (ed Oszmiańska, H.) chap. 1.2.2. <http://books.google.com/books?id=mUHNAQAACAAJ> (Art Stations Foundation, Poznań, Poland, 2009) (cit. on p. 30).
27. Rydzak, J. *Zbig Rybczyński, Oscar-Winning Filmmaker* interview. Arizona, USA, 2014. http://youtube.com/watch?v=071_XgZ4{H}2I (cit. on p. 35).
28. Thoby, M. *About the various projections of the photographic objective lenses. Orthographic fisheye projection* http://michel.thoby.free.fr/Fisheye_history_short/Projections/Variou_s_lens_projection.html (2019) (cit. on p. 31).
29. *Todd AO High-Speed Anamorphic 35mm T1.4 at T2.0log* from The Ultimate Anamorphic Lens Test. ShareGrid, Inc. <https://learn.sharegrid.com/sharegrid-lens-test-todd-ao-anamorphic> (2020) (cit. on p. 35).
30. Tyler, C. W. Straightness and the Sphere of Vision. *Perception* **38**, 1423–1427. doi:10.1068/p3810ed (2009) (cit. on p. 30).
31. Wade, N. J. & Hughes, P. Fooling the Eyes: Trompe LOeil and Reverse Perspective. *Perception* **28**, 1115–1119. doi:10.1068/p281115. [http://wexler.free.fr/library/files/wade%20\(1999\)%20fooling%20the%20eyes.%20trompe%20oeil%20and%20reverse%20perspective.pdf](http://wexler.free.fr/library/files/wade%20(1999)%20fooling%20the%20eyes.%20trompe%20oeil%20and%20reverse%20perspective.pdf) (1999) (cit. on p. 27).
32. Wang, J., Shi, F., Zhang, J. & Liu, Y. A new calibration model of camera lens distortion. *Pattern Recognition* **41**, 607–615. doi:10.1016/j.patcog.2007.06.012. <http://dia.fi.upm.es/~lbaumela/Vision13/PapersCalibracion/wang-PR208.pdf> (2008) (cit. on p. 26).
33. Wikipedia, contributors. *Robert Barker (painter)*. *Biography* Wikimedia Foundation, Inc. [http://en.wikipedia.org/w/index.php?title=Robert_Barker_\(painter\)&oldid=907715733#Biography](http://en.wikipedia.org/w/index.php?title=Robert_Barker_(painter)&oldid=907715733#Biography) (2019) (cit. on p. 35).

© 2020 Jakub Maksymilian Fober (the Author). The Author provides this document (the Work) under the Creative Commons CC BY-ND 3.0 license available online. To view a copy of this license, visit <https://creativecommons.org/licenses/by-nd/3.0/> or send a letter to Creative Commons, PO Box 1866, Mountain View, CA 94042, USA. The Author further grants permission for reuse of images and text from the first page of the Work, provided that the reuse is for the purpose of promoting and/or summarizing the Work in scholarly venues and that any reuse is accompanied by a scientific citation to the Work.



```
1 // Pixel step
2 float pxstep(float gradient)
3 { return clamp(gradient / fwidth(gradient) + 0.5, 0.0, 1.0); }
4
5 // Binary pixel step
6 bool bpxstep(float gradient)
7 { return gradient > -fwidth(gradient) * 0.5; }
8
9 // Partial derivative calculation, can be saved as a texture
10 float get_map_delta(vec3 visual_sphere)
11 {
12     visual_sphere = fwidth(visual_sphere);
13     // Reciprocal of perspective map maximum partial derivative
14     return 1.0 / max(max(visual_sphere.x, visual_sphere.y),
15                     visual_sphere.z);
16 }
17 // Pixel step with derivative in texture
18 float gpxstep(float gradient, float map_del)
19 { return clamp(gradient * map_del + 0.5, 0.0, 1.0); }
20
21 // Binary pixel step with derivative in texture
22 bool gbpxstep(float gradient, float map_del)
23 { return gradient > -0.5 / map_del; }
```

Listing 1: Aliasing-free step function in GLSL.

```

1 float dot(vec3 vector) { return dot(vector, vector); }
2
3 // Once per polygon
4 vec4 getMiterVector(mat3 triangle)
5 {
6     // Project polygon onto sphere
7     triangle[0] = normalize(triangle[0]); // Vertex A
8     triangle[1] = normalize(triangle[1]); // Vertex B
9     triangle[2] = normalize(triangle[2]); // Vertex C
10
11     // Get polygon sides squared
12     vec3 barycenter = vec3(
13         dot(triangle[1]-triangle[2]),
14         dot(triangle[2]-triangle[0]),
15         dot(triangle[0]-triangle[1])
16     );
17     // Get circumcenter
18     barycenter *= barycenter.gbr+barycenter.brg-barycenter;
19     // Get smallest circle vector
20     if (barycenter.s <= 0.0)
21         barycenter = 0.5*(triangle[1]+triangle[2]);
22     else if (barycenter.t <= 0.0)
23         barycenter = 0.5*(triangle[2]+triangle[0]);
24     else if (barycenter.p <= 0.0)
25         barycenter = 0.5*(triangle[0]+triangle[1]);
26     else
27         barycenter = (barycenter.s*triangle[0]+barycenter.t*
28             triangle[1]+barycenter.p*triangle[2])
29             /(barycenter.s+barycenter.t+barycenter.p);
30     // Smallest circle center vector and radius
31     return vec4(normalize(barycenter), length(barycenter));
32 }

```

Listing 2: Polygon miter mask function in GLSL, where matrix *triangle* represents vertices in camera-space.

```

1  vec3 normal(vec3 A, vec3 B)
2  { return normalize(cross(A, B) ); }
3
4  // Once per polygon
5  mat3 getRasterMatrix(mat3 triangle)
6  {
7      return mat3(
8          normal(triangle[0], triangle[1]),
9          normal(triangle[1], triangle[2]),
10         normal(triangle[2], triangle[0])
11     );
12 }
13
14 // Once per fragment pixel
15 float getPolygonOutline(vec3 visual_sphere, mat3 raster, vec4 miter
16 )
17 {
18     vec4 masks;
19     masks.rgb = visual_sphere*raster;
20     masks.a = dot(visual_sphere, miter.xyz)-miter.w;
21
22     float outline = pxstep(masks[0]);
23     for (int i=1; i<4; i++)
24         outline = min(pxstep(masks[i]), outline);
25
26     return outline;
27 }

```

Listing 3: Aliasing-free rasterization function in GLSL. Function *pxstep()* is described in listing 1 on page 45.

```

1  // Once per region
2  bool getPolygonRegion(vec3 visual_sphere, mat3 raster)
3  {
4      vec3 masks = visual_sphere*raster;
5      // extend outline
6      masks += fwidth(masks)*0.5;
7
8      bool outline = masks[0]>0.0;
9      for (int i=1; i<4; i++)
10         outline &= masks[i]>0.0;
11
12     return outline;
13 }

```

Listing 4: Binary (jagged) step rasterization function in GLSL. This version produces aliased result, suitable for low-resolution fragment region evaluation.

```

1 float dot(vec3 vector) { return dot(vector, vector); }
2
3 // Once per polygon
4 vec3 getHardNormal(mat3 triangle)
5 { return cross(triangle[0]-triangle[1], triangle[2]-triangle[1]); }
6
7 // Once per fragment pixel
8 vec4 getBarCoord(vec3 visual_sphere, mat3 triangle, vec3
   hard_normal)
9 {
10     // Extend onto polygon plane intersection
11     float depth = dot(triangle[0], hard_normal)/dot(visual_sphere,
   hard_normal);
12     visual_sphere *= depth;
13
14     for (int i=0; i<3; i++)
15         triangle[i] -= visual_sphere;
16
17     return vec4(vec3(
18         dot(cross(triangle[2], triangle[1]), hard_normal),
19         dot(cross(triangle[0], triangle[2]), hard_normal),
20         dot(cross(triangle[1], triangle[0]), hard_normal)
21     )/dot(hard_normal), depth);
22 }

```

Listing 5: Barycentric vector function with hard normal and depth function for fragment-data interpolation in GLSL.


```

1  float lpxstep(float scalar)
2  { return 1.0-min(abs(scalar)/fwidth(scalar), 1.0); }
3
4  // Once per polygon side
5  vec4 getLineVector(vec3 A, vec3 B)
6  {
7      // Project vertices onto sphere
8      A = normalize(A); B = normalize(B);
9      vec3 line_center = (A+B)*0.5;
10     return vec4(normalize(line_center), length(line_center) );
11 }
12
13 // Once per polygon side
14 vec3 normal(vec3 A, vec3 B)
15 { return normalize(cross(A, B) ); }
16
17 // Once per line's pixel
18 float getLineSegment(vec3 vis_sphere , vec3 normal, vec4 line_vec)
19 {
20     // Great circle
21     float line = lpxstep(dot(vis_sphere , normal) );
22     // Apply segment mask
23     return line*pxstep(dot(vis_sphere , line_vec.xyz)-line_vec.w);
24 }

```

Listing 6: Aliasing-free line segment rasterization function in GLSL. Function **pxstep()** can be found in listing 1 on page 45.

```

1  bool getAliasedLineSegment(vec3 vis_sphere , vec3 normal, vec4
   line_vec)
2  {
3     float great_circle = dot(vis_sphere , normal);
4     // Binary line-step operation
5     bool line = fwidth(great_circle)-abs(2.0*great_circle) > 0.0;
6     // Apply segment mask
7     return line && dot(vis_sphere , line_vec.xyz)-line_vec.w > 0.0;
8  }

```

Listing 7: Binary (jagged) line segment rasterization function in GLSL.

```

1 float dot(vec3 vector) { return dot(vector, vector); }
2 float sq(float scalar) { return scalar*scalar; }
3 vec3 normal(vec3 A, vec3 B)
4 { return normalize(cross(A, B) ); }
5
6 // Once per particle's pixel
7 float getParticleMask(vec3 visual_sphere, vec4 particle)
8 {
9     return pxstep(dot(visual_sphere, particle.xyz)
10                  -sqrt(1.0-sq(particle.w)/dot(particle.xyz) ) );
11 }
12
13 // Once per particle, per frame
14 mat2x3 getParticleTexCoordMatrix(vec4 particle)
15 {
16     vec3 X = normalize(vec3(particle.z, 0.0, -particle.x) );
17     return mat2x3(X, normal(X, particle.xyz) );
18 }
19
20 // Once per particle's pixel
21 vec2 getParticleTexCoord(vec3 visual_sphere, mat2x3 particle_mat,
22                          vec4 particle)
23 { return (visual_sphere*particle_mat)*length(particle.xyz)/particle
24          .w*0.5+0.5; }

```

Listing 8: Particle rasterization function in GLSL. Function *pxstep()* can be found in listing 1 on page 45.

```

1 // Returns fragment mask occluded by render buffer mask
2 float clipFragment(float fragMask, float maskBuffer)
3 { return min(fragMask, 1.0-maskBuffer); }
4
5 // Combines current fragment mask with the buffer
6 float combineMaskPass(float fragClip, float maskBuffer)
7 { return fragClip+maskBuffer; }
8
9 // Combines current fragment depth with the buffer
10 float combinePass(float fragClip, float fragDepth, float
11                  depthBuffer)
12 { return fragClip*fragDepth+depthBuffer; }
13
14 // Combines current fragment texture coordinates with the buffer
15 vec2 combinePass(float fragClip, vec2 fragCoord, vec2 texBuffer)
16 { return fragClip*fragCoord+texBuffer; }
17
18 // Combines current fragment normal with the buffer
19 vec3 combinePass(float fragClip, vec3 fragNormal, vec3 normBuffer)
20 { return fragClip*fragNormal+normBuffer; }

```

Listing 9: Fragment data occlusion and buffer merging, for front-to-back rasterization, in GLSL.

```

1 // Convert texture coordinates to screen coordinates
2 vec2 getScreenCoord(vec2 texCoord, float aspectRatio, int fovType)
3 {
4     // FOV type:
5     // 0 - horizontal
6     // 1 - diagonal
7     // 2 - vertical
8     // 3 - horizontal 4x3
9
10    // Center coordinates
11    vec2 scrCoord = texCoord * 2.0 - 1.0;
12    // Correct aspect ratio
13    if (fovType == 0) // Horizontal
14        scrCoord.y /= aspectRatio;
15    else // Vertical, diagonal, or 4x3
16    {
17        scrCoord.x *= aspectRatio;
18        // Diagonal or 4x3
19        if (fovType == 1) // Diagonal
20            scrCoord *= inversesqrt(aspectRatio * aspectRatio + 1.0);
21        else if (fovType == 3) // 4x3
22            scrCoord /= 4.0 / 3.0;
23    }
24
25    return scrCoord;
26 }
27
28 // Convert screen coordinates to texture coordinates
29 vec2 getTextureCoord(vec2 scrCoord, float aspectRatio, int fovType)
30 {
31     // FOV type:
32     // 0 - horizontal
33     // 1 - diagonal
34     // 2 - vertical
35     // 3 - horizontal 4x3
36
37     // Map aspect ratio to square
38     if (fovType == 0) // Horizontal
39         scrCoord.y *= aspectRatio;
40     else // Vertical, diagonal, or 4x3
41     {
42         scrCoord.x /= aspectRatio;
43         // Diagonal or 4x3
44         if (fovType == 1) // Diagonal
45             scrCoord *= sqrt(aspectRatio * aspectRatio + 1.0);
46         else if (fovType == 3) // 4x3
47             scrCoord *= 4.0 / 3.0;
48     }
49
50     // Map to corner
51     return scrCoord * 0.5 + 0.5;
52 }

```

Listing 10: Texture to screen coordinates transformation with aspect ratio and FOV conversion, in GLSL.

```

1 void limits(inout float k, inout float l, inout float s, inout
   float fov)
2 {
3     k = clamp(k, -1.0, 1.0);
4     l = clamp(l, 0.0, 1.0);
5     s = clamp(s, 0.8, 1.0);
6     // Field of view in degrees
7     float fov_max = (k > 0.0 ? 179.0 : 180.0) / max(abs(k), 0.5);
8     fov = clamp(fov, 1.0, fov_max);
9 }

```

Listing 11: Function for range limiting of universal perspective parameters (k , l , s and Ω) in GLSL.

```

1  vec2 getViewCoord(vec2 tex_coord , float aspect , int fov_type)
2  {
3      tex_coord.xy = 2.0*tex_coord.st - 1.0;
4      switch (fov_type)
5      {
6          default: // horizontal FOV (type 1)
7              tex_coord.y /= aspect;
8              break;
9          case 2: // diagonal FOV (type 2)
10             tex_coord.xy /= length(vec2(aspect , 1.0) );
11          case 3: // vertical FOV (type 3) and type 2 final step
12             tex_coord.x *= aspect;
13             break;
14          case 4: // 4x3 horizontal FOV (type 4)
15             tex_coord.xy *= vec2(0.75*aspect , 0.75);
16             break;
17      }
18      return tex_coord;
19  }
20
21 vec3 getPerspectiveMap(vec2 view_coord , float fov , float k , float l
22 , float s)
23 {
24     float halfOmega = radians(fov*0.5);
25     float R = length(vec2(view_coord.x , l*view_coord.y) );
26
27     float theta;
28     if (k>0.0) theta = atan(tan(k*halfOmega)*R)/k;
29     else if (k<0.0) theta = asin(sin(k*halfOmega)*R)/k;
30     else theta = halfOmega*R;
31
32     view_coord.y /= l*(1.0-s)+s;
33     return normalize(
34         vec3(view_coord*sin(theta)/R , cos(theta) )
35     );

```

Listing 12: Visual sphere vector $\hat{v} \in [-1, 1]^3$ function from texture coordinates $\vec{f} \in [0, 1]^2$ in GLSL, for universal-perspective system.

```

1  vec3 getRectilinearMap(vec2 tex_coord , float aspect , float fov , int
   fov_type)
2  {
3      vec3 direction = vec3(
4          2.0*tex_coord -1.0, // map to range [-1,1]
5          1.0/ tan(0.5*radians(fov) )
6      );
7      switch (fov_type)
8      {
9          default: // horizontal FOV (type 1)
10         direction.y /= aspect;
11         break;
12         case 2: // diagonal FOV (type 2)
13         direction.xy /= length(vec2(aspect , 1.0) );
14         case 3: // vertical FOV (type 3) and type 2 final step
15         direction.x *= aspect;
16         break;
17     }
18
19     return normalize(direction);
20 }

```

Listing 13: Rectilinear perspective visual-sphere vector $\hat{v} \in [-1, 1]^3$ from texture coordinates $\vec{f} \in [0, 1]^2$ in GLSL.

```

1  float getPanormaAspect(float horizontal_fov , float height)
2  { return radians(horizontal_fov)/height; }
3
4  vec3 getPanoramaMap(vec2 tex_coord , float horizontal_fov , float
   height)
5  {
6      tex_coord.xy = vec2(horizontal_fov , height)*(tex_coord.st -0.5);
7
8      return normalize(vec3(
9          sin(tex_coord.x) ,
10         tex_coord.y ,
11         cos(tex_coord.x)
12     ));
13 }

```

Listing 14: Curved panorama perspective visual-sphere vector $\hat{v} \in [-1, 1]^3$ from texture coordinates $\vec{f} \in [0, 1]^2$ in GLSL.

```

1  vec4 getDomeMap(vec2 tex_coord, float compression, float tilt,
   float offset)
2  {
3      tex_coord.xy = vec2(
4          2.0*tex_coord.s-1.0,
5          1.0-2.0*tex_coord.t
6      );
7      float R = length(tex_coord);
8      float theta = R*radians(compression+90.0);
9
10     vec4 perspective_map = vec4(
11         tex_coord*sin(theta)/R,
12         cos(theta),
13         1.0-R
14     ).xyzw;
15     perspective_map.a = clamp(perspective_map.a
16         /fwidth(perspective_map.a), 0.0, 1.0);
17
18     perspective_map.z += offset;
19     perspective_map.xyz = normalize(perspective_map.xyz);
20
21     tilt = radians(tilt);
22     vec2 rotation = vec2(sin(tilt), cos(tilt) );
23     perspective_map.xyz *= mat3(
24         vec3(1.0, 0.0, 0.0),
25         vec3(0.0, rotation[1], -rotation[0]),
26         vec3(0.0, rotation[0], rotation[1])
27     );
28
29     return perspective_map;
30 }

```

Listing 15: Full dome visual-sphere vector $\hat{v} \in [-1, 1]^3$ from texture coordinates $\vec{f} \in [0, 1]^2$ in GLSL.

```

1  vec3 getEquirectangularMap(vec2 tex_coord)
2  {
3      tex_coord.x = 2.0*tex_coord.s-1.0;
4      tex_coord.xy *= radians(180.0);
5
6      vec2 sine = sin(tex_coord);
7      vec2 cosine = cos(tex_coord);
8
9      return vec3(sine.x*sine.y, -cosine.y, cosine.x*sine.y);
10 }

```

Listing 16: Equirectangular projection visual-sphere vector $\hat{v} \in [-1, 1]^3$ from texture coordinates $\vec{f} \in [0, 1]^2$ in GLSL.

```

1 float dot(vec3 vector) { return dot(vector, vector); }
2 float sq(float scalar) { return scalar*scalar; }
3 float pxstep(float scalar)
4 { return clamp(scalar/fwidth(scalar), 0.0, 1.0); }
5
6 vec4 getMirrorDomeMap(vec3 mirror_normal, vec3 projector_map, mat3
  projector_rot, vec3 projector_pos, float dome_radius, vec3
  dome_pos)
7 {
8   vec3 reflection = reflect(projector_map, mirror_normal)*
  projector_rot;
9   vec3 mirror_surface = mirror_normal*projector_rot;
10  dome_pos -= mirror_surface; // set current mirror surface as origin
11
12  // Get reflection length to dome intersection
13  float length = dot(reflection.xyz, dome_pos.xyz);
14  length += sqrt( dome_radius*dome_radius-dot(dome_pos.xyz-length
  *reflection.xyz) );
15
16  return vec4(
17    (length*reflection.xyz-dome_pos.xyz)/dome_radius,
18    length+length(mirror_surface.xyz-projector_pos.xyz)
19  );
20 }
21
22 vec4 processMirrorDomeMask(vec2 tex_coord, vec3 dome_pos)
23 {
24   vec2 pixSize = 1.0/ sizeof(MirrorDomeMap);
25   vec4 mirror_dome = texture(MirrorDomeMap, tex_coord);
26
27   // Get mirror-bounds mask
28   float alpha = texture(MirrorNormalPass, tex_coord).a;
29   // Generate reflected-dome-bounds mask
30   alpha *= pxstep(mirror_dome.z); // half dome clip
31   alpha *= pxstep(mirror_dome.y+dome_pos.y); // bottom clip
32
33   // Get maximum incident length for normalization
34   float max_incident = 0.0;
35   for (int y=0; y<sizeof(MirrorDomeMap).y; y++)
36   for (int x=0; x<sizeof(MirrorDomeMap).x; x++)
37     max_incident = max(
38       max_incident,
39       alpha*texture(MirrorDomeMap, vec2(x,y)*pixSize).w
40     );
41
42   // Combine normalized brightness mask
43   alpha *= sq(mirror_dome.w/ max_incident);
44
45   return vec4(mirror_dome.xyz, alpha);
46 }

```

Listing 17: Mirror-dome visual-sphere vector $\hat{v} \in [-1, 1]^3$ from mirror normal-pass, as seen through projector in GLSL.


```

1  vec3 getProjectionMap(vec2 tex_coord, vec3 view_pos, mat3 view_mat)
2  {
3      vec3 world_pos = texture(WorldPos, tex_coord).xyz;
4      return normalize(world_pos-view_pos)*view_mat;
5  }
6
7  float getBrightnessMask(vec2 tex_coord)
8  {
9      vec2 pixSize = 1.0/ sizeof(WorldPos);
10
11     float max_dist2 = 0.0;
12     for (int y=0; y<sizeof(WorldPos).y; y++)
13     for (int x=0; x<sizeof(WorldPos).x; x++)
14     {
15         vec3 incident = texture(WorldPos, pixSize*vec2(x,y)).xyz
16         max_dist2 = max(max_dist2, dot(incident, incident));
17     }
18
19     vec3 incident = texture(WorldPos, tex_coord).xyz;
20     return dot(incident, incident)/max_dist2;
21 }

```

Listing 18: Visual sphere vector $\hat{v} \in [-1, 1]^3$ function from world-position pass as seen through projector in GLSL, for projection mapping.

```

1  vec3 getScreenArrayMap(vec2 tex_coord, int n, float horizontal_fov,
   float aspect)
2  {
3      horizontal_fov = radians(horizontal_fov);
4      float index = floor(n*tex_coord.s)-0.5*n+0.5;
5      // Get single screen coordinates
6      vec3 direction = normalize(vec3(
7          2.0*fract(n*tex_coord.s)-1.0,
8          n*(2.0*tex_coord.t-1.0)/aspect,
9          1.0/tan(horizontal_fov*0.5)
10     ));
11     // Rotate each screen individually
12     horizontal_fov *= index;
13     vec2 rotation = vec2(
14         sin(horizontal_fov),
15         cos(horizontal_fov)
16     );
17
18     return direction*mat3(
19         rotation[1], 0.0, rotation[0],
20         0.0, 1.0, 0.0,
21         -rotation[0], 0.0, rotation[1]
22     );
23 }

```

Listing 19: Visual sphere vector $\hat{v} \in [-1, 1]^3$ function from texture coordinates $\vec{f} \in [0, 1]^2$ in GLSL, for n -screen-array perspective.

```

1  vec3 getVRMap(vec2 tex_coord, float ipd, float vertical_fov, float
   k1, float k2, float aspect)
2  {
3      float index = sign(tex_coord.s-0.5);
4      // Convert to stereoscopic coordinates
5      tex_coord.xy = 2.0*vec2(fract(2.0*tex_coord.s), tex_coord.t)
6         -1.0;
7      // Convert to view coordinates with IPD offset (in screen-width ratio)
8      tex_coord.x = (tex_coord.x+index*(1.0-2.0*ipd)) *0.5*aspect;
9      // Apply lens distortion
10     float R2 = dot(tex_coord, tex_coord); // Radius squared
11     tex_coord *= (1.0+k1*R2+k2*R2*R2)/(1.0+k1+k2); // Vertical
12         normalization
13
14     // Output incident vector
15     return normalize(vec3(
16         tex_coord,
17         1.0/tan(radians(vertical_fov)*0.5)
18     ));
19 }

```

Listing 20: VR visual-sphere vector $\hat{v} \in [-1, 1]^3$ from texture coordinates $\vec{f} \in [0, 1]^2$ in GLSL. The *ipd* variable is expressed in screen-width scale.

```

1  vec3 applyLensDistortion(vec2 tex_coord, float k1, float k2, float
2  {
3      float diagonal = inversesqrt( aspect*aspect+1.0);
4      // Center coordinates
5      tex_coord.xy = 2.0*tex_coord.st -1.0;
6      // Correct aspect
7      tex_coord.x *= aspect;
8      // Normalize diagonally
9      tex_coord *= diagonal;
10
11     vec2 distort_coord = tex_coord;
12     // Get radius squared
13     float R2 = dot(tex_coord, tex_coord);
14     // Radial distortion
15     distort_coord *= k1*R2+(k2*(R2*R2)+1.0);
16     // Thin prism distortion
17     distort_coord += tex_coord*dot(vec2(p1, p2), tex_coord);
18     // Decentering distortion
19     distort_coord += vec2(q1, q2)*R2;
20
21     // Lens-distorted view-coordinates
22     return distort_coord;
23 }

```

Listing 21: Lens distortion function for transformation of texture coordinates $\vec{f} \in [0, 1]^2$ to view coordinates $\vec{f}' \in \mathbb{R}^2$ in GLSL.